Antibacterial T6SS effectors with a VRR-Nuc domain induce target cell death via DNA Double-Strand Breaks

Julia Takuno Hespanhol[1,a], Daniel Enrique Sanchez Limache[1,a], Gianlucca Gonçalves Nicastro[1], Liam Mead[2], Edgar Enrique Llontop[3], Gustavo Chagas Santos[1], Chuck Shaker Farah[3], Robson Francisco de Souza[1], Rodrigo da Silva Galhardo[1], Andrew Lovering[2], Ethel Bayer Santos[1]*

1. Departamento de Microbiologia, Instituto de Ciências Biomédicas, Universidade de São Paulo, São Paulo 05508-900, Brazil.

2. Department of Biosciences, University of Birmingham, Birmingham, UK.

3. Departamento de Bioquímica, Instituto de Química, Universidade de São Paulo, São Paulo 05508-000, Brazil.

* Corresponding author: ebayersantos@usp.br

[a] These authors contributed equally to this work.

Running title: The antibacterial SPI-22 T6SS uses VRR-Nuc-containing effectors.

Abstract

The T6SS (Type VI secretion System) secretes antibacterial effectors into target competitors. *Salmonella* spp. encode five phylogenetically distinct T6SSs. Here we characterize the function of the SPI-22 T6SS of *S. bongori*, showing that it has antibacterial activity. We identify a group of antibacterial T6SS effectors (TseV1-4) containing an N-terminal PAAR-like domain and a C-terminal VRR-Nuc domain encoded next to cognate immunity proteins that contain the DUF3396 domain (TsiV1-4). TseV2 and TseV3 are toxic when expressed in *Escherichia coli* and bacterial competition assays confirm that TseV2 and TseV3 are secreted by the SPI-22 T6SS. Phylogenetic analysis reveals that TseV1-4 are evolutionarily related to enzymes involved in DNA repair. TseV2 and TseV3 maintained the ability to bind DNA, but instead cause specific DNA double-strand breaks and induce the SOS response in target cells. The crystal structure of the TseV3:TsiV3 complex reveals that the immunity protein likely blocks the effector interaction with the DNA substrate. These results expand our knowledge on the function of *Salmonella* pathogenicity islands, the evolution of toxins used in biological conflicts, and the endogenous mechanism regulating the activity of these toxins.

Keywords: DUF3396/Effectors/SPI-22/T6SS/VRR-Nuc.

Introduction

Bacteria use a series of antagonistic mechanisms to counteract competitors. These processes either require physical contact between attacker and target cells or function in a contact-independent manner via soluble molecules secreted into the medium (Peterson *et al*, 2020). The type VI secretion system (T6SS) is a multi-protein contractile nanomachine evolutionarily related to bacteriophages (Leiman *et al*, 2009). This system is widespread in Gram-negative bacteria and secretes toxic effectors into target cells in a contact-dependent manner (Coulthurst, 2019). The T6SS is composed of three major complexes: the membrane complex, the baseplate and the tail (Nguyen *et al*, 2018). The tail has a spear-like shape and is propelled against target cells upon a contraction event (Wang *et al*, 2017; Salih *et al*, 2018). The tail tube is composed of hexameric rings of Hcp (hemolysin co-regulated protein) capped with a spike composed of a trimer of VgrG (valine-glycine repeat protein G) and a PAAR protein (proline-alanine-alanine-arginine repeats) (Mougous *et al*, 2006; Shneider *et al*, 2013; Renault *et al*, 2018). The effectors secreted via T6SSs associate with Hcp, VgrG or PAAR either directly or indirectly via adaptor proteins (cargo effectors). In addition, so-called evolved effectors are fused to the C-terminus of Hcp, VgrG or PAAR (Cianfanelli *et al*, 2016; Jana & Salomon, 2019). Several isoforms of VgrG, Hcp and PAAR proteins can be encoded in the same bacterial genome, usually outside of the T6SS structural gene cluster (and are thus named orphan proteins). These Hcp, VgrG and PAAR proteins can assemble in different combinations to secrete specific subsets of effectors (Hachani *et al*, 2014; Bondage *et al*, 2016).

T6SSs effectors can target eukaryotic cells, prokaryotic cells or contribute to the acquisition of micronutrients (Coulthurst, 2019). The variety of targets is related to the diversity of biochemical activities of T6SS effectors, which can be nucleases, peptidoglycan hydrolases, lipases, NADases, pore-forming proteins or enzymes that post-

translationally modify target proteins (Jurėnas & Journet, 2021). Antibacterial effectors with nuclease activity are among the most potent weapons used by an attacker to intoxicate target cells. Several T6SS effectors with nuclease activity have been reported including, *Dickeya dadantii* RhsA-CT and RhsB-CT (Koskiniemi *et al*, 2013); *Agrobacterium tumefaciens* Tde1 and Tde2 (Ma *et al*, 2014); *Pseudomonas aeruginosa* PA0099 (Hachani *et al.*, 2014), TseT (Burkinshaw *et al*, 2018) and Tse7 (Pissaridou, 2018); *Serratia marcescens* Rhs2 (Alcoforado Diniz & Coulthurst, 2015); *Escherichia coli* Hcp-ET1, -ET3 and -ET4 (Ma *et al*, 2017a), and Rhs-CT3, -CT4, -CT5, -CT6, -CT7 and -CT8 (Ma *et al*, 2017b); *Acinetobacter baumannii* Rhs2-CT (Fitzsimons *et al*, 2018); *Vibrio parahaemolyticus* PoNe (Jana *et al*, 2019); *Aeromonas dhakensis* TseI (Pei *et al*, 2021); and *Burkholderia gladioli* TseTBg (Yadav *et al*, 2021).

The majority of the nuclease domains mentioned above have been previously predicted by a seminal *in silico* study using comparative genomics (Zhang *et al*, 2012). Among those characterized are Ntox15 (PF15604) (Ma et al., 2014); Ntox30 (PF15532), Ntox34 (PF15606) and Ntox44 (PF15607) (Ma *et al.*, 2017a); Tox-REase-1 (Jana et al., 2019); Tox-REase-3 (PF15647) (Ma *et al.*, 2017a); Tox-REase-5 (PF15648) (Burkinshaw *et al.*, 2018; Yadav *et al.*, 2021); Tox-GHH2 (PF15635) (Hachani *et al.*, 2014; Pissaridou, 2018); HNH (PF01844) (Koskiniemi *et al.*, 2013; Alcoforado Diniz & Coulthurst, 2015; Ma *et al.*, 2017b); Tox-JAB-2 (Ma *et al.*, 2017a); AHH (PF14412) (Ma *et al.*, 2017a; Fitzsimons *et al.*, 2018); and Tox-HNH-EHHH (PF15657) (Pei *et al.*, 2021).

In *Salmonella* species, T6SSs are encoded in five distinct *Salmonella* pathogenicity islands (SPI-6, SPI-19, SPI-20, SPI-21 and SPI-22) acquired by different horizontal gene transfer events (Blondel *et al*, 2009; Bao *et al*, 2019). The *S. enterica* serovar Typhimurium SPI-6 T6SS is involved in competition with the host microbiota and gut colonization (Pezoa *et al*, 2014; Brunet *et al*, 2015; Sana *et al*, 2016; Sibinelli-

Sousa *et al*, 2020); whereas the SPI-19 T6SS of *S.* Gallinarium is involved in survival within macrophages (Blondel *et al*, 2013; Schroll *et al*, 2019). So far, only two T6SS effectors have been characterized in *Salmonella* spp., both targeting peptidoglycan: Tae4 (type VI amidase effector 4) is a gamma-glutamyl-D,L-endopeptidases that cleaves between D-*i*Glu[2] and *m*DAP[3] within the same peptide stem (Russell *et al*, 2012; Benz *et al*, 2013; Zhang *et al*, 2013); and Tlde1 (type VI L,D-transpeptidase effector 1), which exhibits both L,D-carboxypeptidase and L,D-transpeptidase D-amino acid exchange activity, cleaving between *m*DAP[3] and D-Ala[4] of the acceptor tetrapeptide stem or replacing the D-Ala[4] by a noncanonical D-amino acid, respectively (Sibinelli-Sousa *et al.*, 2020).

Herein we report the characterization of the SPI-22 T6SS of *S. bongori*, which displays antibacterial activity. We characterize a group of antibacterial effectors secreted by this system that contain a VRR-Nuc (virus-type replication-repair nuclease) domain (Kinch *et al*, 2005; Iyer *et al*, 2006), named type VI effector VRR-Nuc 1-4 (TseV1-4). These effectors are encoded next to DUF3396-containing proteins, which function as immunity proteins (TsiV1-4) that are specific to each effector. Phylogenetic analysis revealed that TseVs effectors form a clade together with other antibacterial effectors belonging to the PD-(D/E)xK phosphodiesterase superfamily. This toxic clade is phylogenetically related to enzymes containing the VRR-Nuc domain conventionally involved in DNA repair and metabolism. We confirm that TseV2 and TseV3 display DNAse activity, inducing the SOS response with resultant target cell death via DNA double-strand breaks. Our crystal structure of the TseV3:TsiV3 complex reveals that the immunity protein likely impairs effector toxicity by interacting with and occluding its DNA-binding site. Our results provide mechanistic knowledge about a new group of antibacterial toxins that co-opt the VRR-Nuc domain for a previously undescribed role in

bacterial antagonism, and further reveal the mode of neutralization via specific immunity protein complexation.

Results

The SPI-22 T6SS of *S. bongori* has antibacterial activity

The SPI-22 T6SS of *S. bongori* is phylogenetically related to the HSI-III (Hcp secretion island III) T6SS of *Pseudomonas aeruginosa* (amino acid similarity ranging from 26-80%), and the CTS2 (*Citrobacter rodentium* T6SS cluster 2) of *C. rodentium* (amino acid similarity ranging from 63-93%) (Petty *et al*, 2010; Fookes *et al*, 2011) (Fig. 1A). Besides the structural T6SS components encoded within SPI-22, the genome of *S. bongori* NCTC 12419 encodes several orphan proteins comprising two VgrGs (SBG_2715, SBG_3770), four Hcps (SBG_0599, SBG_3120, SBG_3143, SBG_3925), three DUF4150/PAAR-like proteins (SBG_1846, SBG_2718, SBG_2955), two adaptors containing DUF2169 (SBG_1847, SBG_2721), and one adaptor with DUF1795 (SBG_3173) (Fig. 1B).

To analyze whether *S. bongori* SPI-22 T6SS has *bona fide* antibacterial activity, we performed bacterial competition assays using the wild-type (WT) and T6SS null mutant (Δ*tssB/SBG_1238*) strains as attacker cells, and *Escherichia coli* K12 W3110 as prey. Results showed that the prey recovery rate was higher when co-incubation was performed with Δ*tssB* compared to the WT (Fig. 1C). In addition, competition with a Δ*tssB* strain complemented with a plasmid expressing TssB restored the WT phenotype (Fig. 1C). These results show that the SPI-22 T6SS of *S. bongori* is active in the conditions tested and contributes to interbacterial antagonism, thus priming investigation to further characterize this activity.

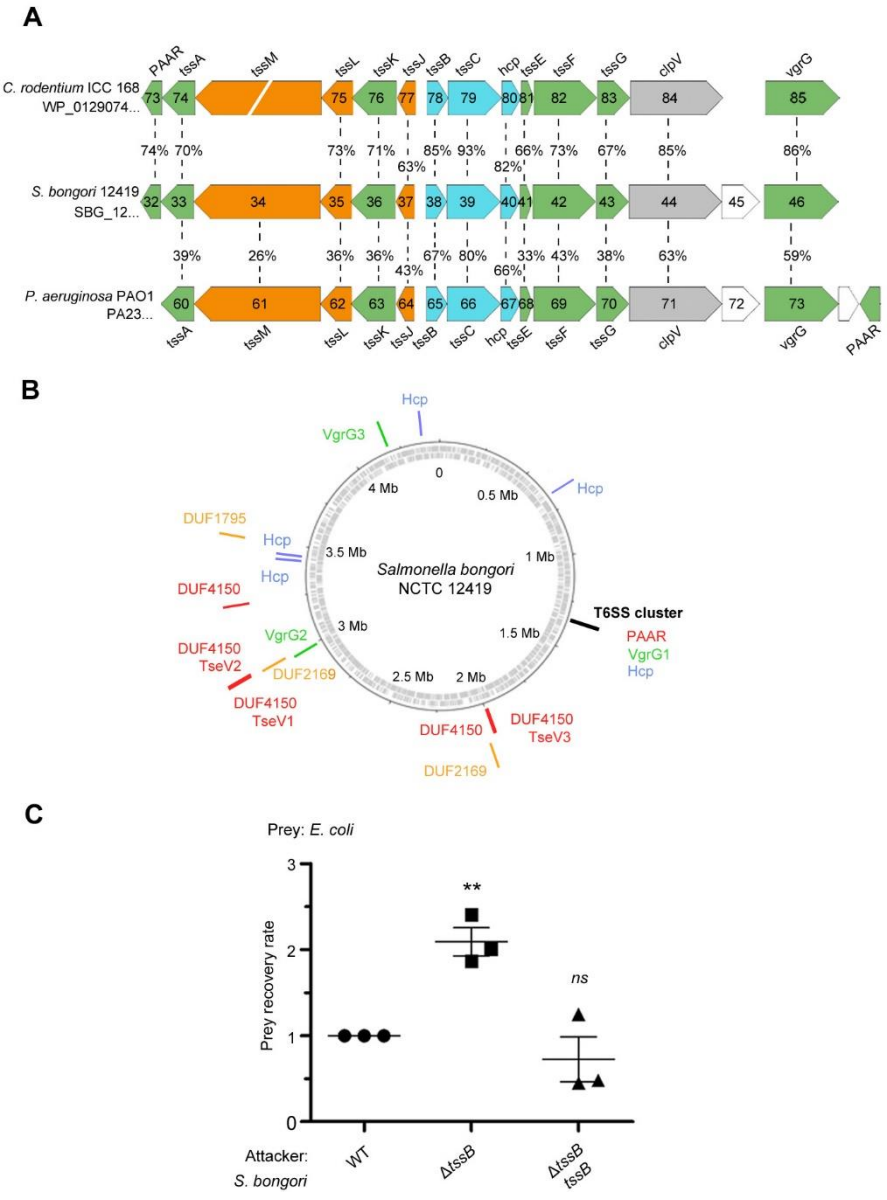

Fig. 1. The *S. bongori* SPI-22 encodes an antibacterial T6SS. (A) Comparison between the SPI-22 T6SS of *S. bongori* with the systems of *C. rodentium* and *P. aeruginosa*. The T6SS proteins forming the three subcomplexes are in colors: membrane components (orange), sheath and inner tube (blue), and baseplate and spike components (green). (B) Representation of the circular genome of *S. bongori* with T6SS components highlighted: the structural cluster is marked by a black line; VgrG proteins are represented by green lines; Hcps are in blue; adaptor proteins are in orange; and PAAR or PAAR-like proteins are in red. TseV1, TseV2 and TseV3 fused to PAAR-like domain are also in red. (C) Bacterial competition assays between *S. bongori* WT, Δ*tssB* and Δ*tssB* complemented with pFPV25.1 *tssB* against *E. coli* in LB-agar incubated for 24 h. The prey recovery rate was calculated by dividing the colony-forming unit (CFU) counts of the output by the input. Data represent the mean ± SD of three independent experiments performed in duplicate and were analyzed through comparison with WT that were normalized to 1. One-way ANOVA followed by Dunnett's multiple comparison test. **$p < 0.01$ and *ns* not significant.

151 **TseV2 and TseV3 are antibacterial SPI-22 T6SS effectors**

152 After verifying that the SPI-22 T6SS has antibacterial activity, we set out to
153 identify the effectors contributing to the antagonistic effect. Initially, we performed *in*
154 *silico* analysis using Bastion6 (Wang *et al*, 2018) to evaluate several candidates (10 genes
155 up- and downstream of all T6SS components) (Fig. 1B) for their probability of being a
156 T6SS effector (cutoff score ≥ 0.5) (data not shown). Two candidates called our attention:
157 SBG_2718 (TseV1) and SBG_2723 (TseV2), which contain an N-terminal PAAR-like
158 domain and a C-terminal VRR-Nuc domain (Fig. 2A) (Kinch *et al.*, 2005; Iyer *et al.*,
159 2006). Both putative effectors are encoded next to pairs of genes encoding DUF3396-
160 containing proteins that resemble putative immunity proteins: SBG_2719/TsiV1.1 and
161 SBG_2720/TsiV1.2, and SBG_2724/TsiV2.1 and SBG_2725/TsiV2.2 (Fig. 2A).
162 Additional BLASTP searches in the genome of *S. bongori* identified two extra VRR-Nuc-
163 containing proteins (SBG_1841/TseV3 and SBG_1828/TseV4), but only one of them
164 encoding an N-terminal PAAR-like domain (SBG_1841). Similarly, SBG_1828 and
165 SBG_1841 are encoded upstream of a DUF3396-containing protein (SBG_1829/TsiV4
166 and SBG_1842/TsiV3) (Fig. 2A).

167 To analyze whether these proteins comprise four effector-immunity pairs, we
168 cloned these genes into compatible vectors under the control of different promoters. To
169 evaluate the toxicity of TseV1-4 upon expression in *E. coli*, the C-terminal regions of
170 TseV1-3 and the full-length TseV4 were cloned into the pBRA vector under the control
171 of the P_{BAD} promoter (inducible by L-arabinose and repressed by D-glucose). The
172 putative immunity proteins were cloned into the pEXT22 vector under the control of the
173 P_{TAC} promoter, which is inducible by isopropyl β-D-1-thiogalactopyranoside (IPTG). *E.*
174 *coli* strains carrying different combinations of pBRA and pEXT22 were serially diluted
175 and spotted onto LB agar plates containing either 0.2% D-glucose or 0.2% L-arabinose

176 plus 200 μM IPTG (Fig. 2B). Results showed that TseV2 and TseV3 are toxic in the
177 cytoplasm of *E. coli*, whereas TseV1 and TseV4 do not confer toxicity (Fig. 2B). Co-
178 expression of TseV2 with either TsiV2.1 or TsiV2.2 revealed that only the first immunity
179 protein neutralizes TseV2 toxicity (Fig. 2B). Similarly, the toxic effect of TseV3 can be
180 neutralized by co-expression with TsiV3 (Fig. 2B). Co-expression of TseV2 and TseV3
181 with all combinations of immunity proteins (TsiV1.1, TsiV1.2, TsiV2.1, TsiV2.2, TsiV3
182 and TsiV4) revealed that the effectors are neutralized only by the specific cognate
183 immunity protein (Fig. S1). The effect of TseV2 and TseV3 on cell growth was also
184 analyzed in liquid media by measuring the $OD_{600ηm}$ of *E. coli* carrying pBRA TseV2 or
185 TseV3 (Fig. 2C). Under these conditions, bacteria grew normally in media containing D-
186 glucose; but once L-arabinose was added, the culture stopped growing, and the $OD_{600ηm}$
187 stabilized (Fig. 2C).

188 We performed time-lapse microscopy to evaluate growth and morphology of
189 individual *E. coli* cells harboring pBRA TseV2 or TseV3. Bacteria grew normally when
190 incubated in LB agar pads containing 0.2% D-glucose (repressed) over a time frame of 8
191 h (Fig. 2D, Movies S1, S3). However, in the presence of 0.2% L-arabinose (induced)
192 bacteria did not grow and remained mostly morphologically unaltered – displaying a
193 modest increase in cell length (Fig. 2D, Movies S2, S4).

194 To verify whether TseV2 and TseV3 are SPI-22 T6SS substrates, we performed
195 bacterial competition assays using *S. bongori* WT and Δ*tssB* (attacker) versus *S. bongori*
196 lacking either TsiV2.1/2.2 (Δ*tseV2/tsiV2.1/2.2)* or TsiV3 (Δ*tseV3/tsiV3)* as prey (Fig. 2E).
197 Results demonstrated that the prey recovery rate was higher when prey cells were co-
198 incubated with Δ*tssB* compared to WT (Fig. 2E). Complementation of preys with a
199 plasmid encoding either TsiV2.1 or TsiV3 increased the prey recovery rate, showing that

prey became immune to the TseV2 and TseV3-induced toxicity (Fig. 2E). These results confirm that TseV2 and TseV3 are antibacterial effectors secreted by the SPI-22 T6SS.

As TseV2 and TseV3 contain an N-terminal PAAR-like domain, which interacts with VgrG during T6SS assembly and effector secretion (Shneider *et al.*, 2013), we decided to determine which of the three VgrG proteins encoded in *S. bongori* genome (Fig. 1B, 2A) were responsible for the secretion of TseV2 and TseV3. To shed light on this matter, we performed bacterial competition assays using *S. bongori* WT, Δ*tssB*, Δ*vgrG1* (SBG_1246), Δ*vgrG2* (SBG_2715) or Δ*vgrG3* (SBG_3770) (attacker) versus Δ*tseV2/tsiV2.1/2.2* or Δ*tseV3/tsiV3* (prey) (Fig. 2F). The prey recovery rate of Δ*tseV2/tsiV2.1/2.2* increased when this strain was co-incubated with Δ*vgrG2*, suggesting that VgrG2 is responsible for secreting TseV2 into target cells (Fig. 2F). Conversely, the prey recovery rate of Δ*tseV3/tsiV3* increased when this strain was co-incubated with Δ*vgrG3*, suggesting that VgrG3 is responsible for secreting TseV3 into target cells (Fig. 2F). VgrG2 and VgrG3 are 96.9% identical in their N-terminal region ($VgrG2_{1\text{-}565}$ and $VgrG3_{1\text{-}545}$) but display a distinct C-terminal domain with only 26% identity ($VgrG2_{566\text{-}709}$ and $VgrG3_{546\text{-}728}$) (Fig. S2), thus suggesting that this region is responsible for cargo selection (Liang *et al*, 2021). Together, these results show that each effector has its own mechanism of secretion, which is dependent on distinct VgrGs.

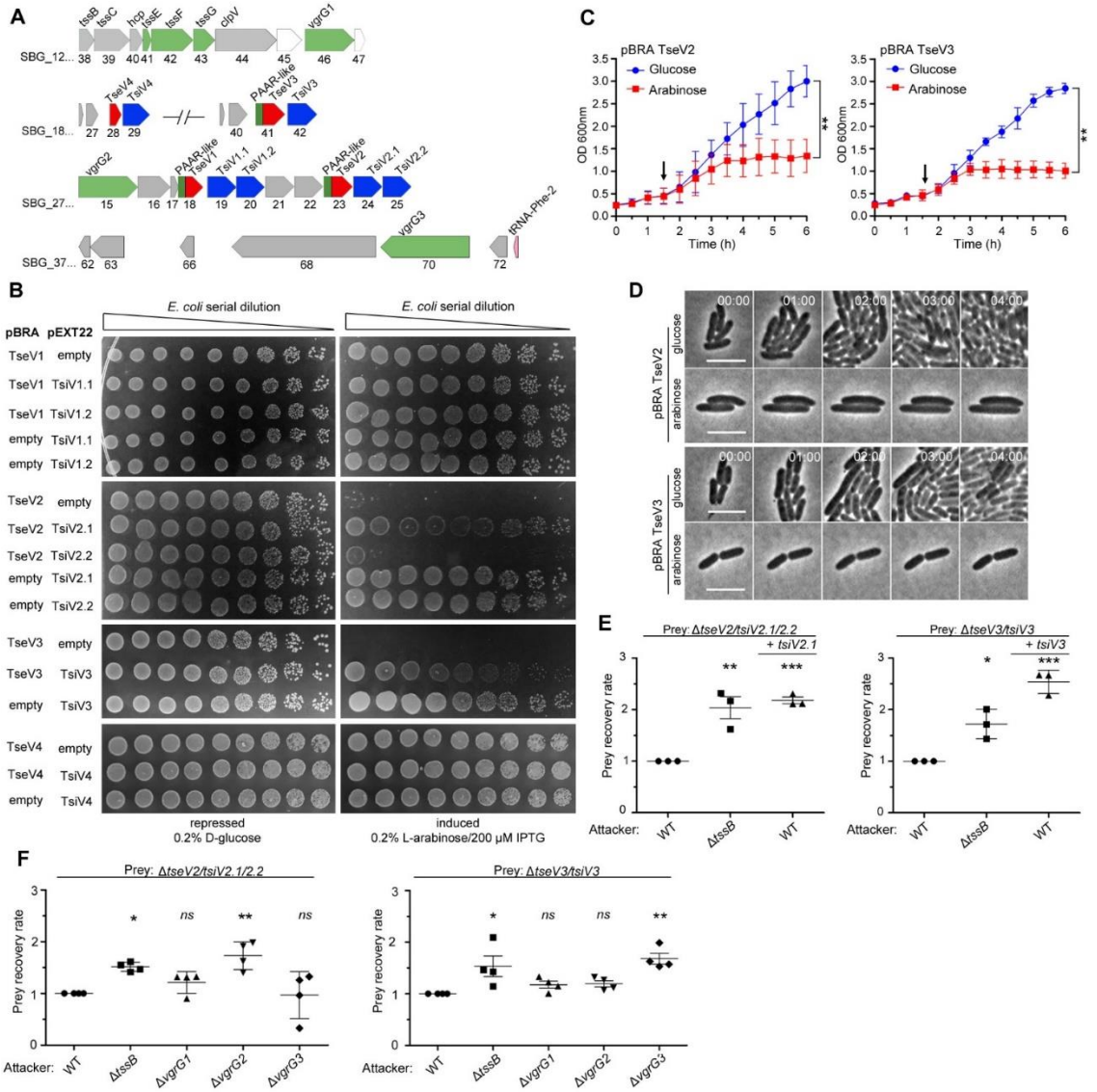

Fig. 2. TseV2 and TseV3 are antibacterial SPI-22 T6SS effectors. (A) Scheme of the genomic region containing VgrGs and TseV/TsiV effector/immunity pairs. VRR-Nuc domain (red), PAAR-like domain (dark green), VgrG (light green), and DUF3396-containing immunities (blue). (B) *E. coli* toxicity assay. Serial dilutions of *E. coli* containing pBRA and pEXT22 constructs, as indicated, spotted onto LB agar plates, and grown for 20 h. Images are representative of three independent experiments. (C) Growth curve of *E. coli* harboring pBRA TseV2 or TseV3 before and after toxin induction by the addition of 0.2% L-arabinose (arrow). Results represent the mean ± SD of three independent experiments performed in duplicate. **p < 0.01 (Student's *t* test). (D) Time-lapse microscopy of *E. coli* carrying either pBRA TseV2 or pBRA TseV3 grown on LB-agar pads containing either 0.2% D-glucose (repressed) or 0.2% L-arabinose (induced). Scale bar: 5 µm. Timestamps in hh:mm. (E) Bacterial competition assay using *S. bongori* WT, Δ*tssB* and Δ*tssB* complemented with pFPV25.1 *tssB* against *S. bongori* Δ*tseV2/tsiV2.1/tsiV2.2* or Δ*tseV3/tsiV3* complemented or not with pFPV25.1 *tsiV2.1* or pFPV25.1 *tsiV3*. Strains were co-incubated for 20 h (Δ*tseV2/tsiV2.1/tsiV2.2*) or 6 h (Δ*tseV3/tsiV3*) prior to measuring CFU counts. The prey recovery rate was calculated by dividing the CFU of the output by the input. Data represent the mean ± SD of three independent experiments performed in duplicate and were analyzed through comparison with WT that were

normalized to 1. One-way ANOVA followed by Dunnett's multiple comparison test. *p < 0.05, **p < 0.01 and ***p < 0.001. (F) Bacterial competition assay using *S. bongori* WT, Δ*tssB*, Δ*vgrG1*, Δ*vgrG2* or Δ*vgrG3* against *S. bongori* Δ*tseV2/tsiV2.1/tsiV2.2* or Δ*tseV3/tsiV3*. Strains were co-incubated for 20 h prior to measuring CFU counts. Prey recovery rate was calculated as in (E). Data represent the mean ± SD of four independent experiments performed in duplicate. One-way ANOVA followed by Dunnett's multiple comparison test. *p < 0.05, **p < 0.01 and *ns* (not significant).

VRR-Nuc-containing effectors are evolutionarily related to Holliday junction resolvases and enzymes involved in DNA repair.

TseV2 and TseV3 contain a VRR-Nuc domain at their C-terminus, which was initially annotated as DUF994 (Kinch *et al.*, 2005) and later renamed VRR-Nuc due to its association with enzymes linked to DNA metabolism (Iyer *et al.*, 2006). VRR-Nuc-containing proteins are found in a wide range of organisms, including bacteria, bacteriophages, fungi, and eukaryotes (Iyer *et al.*, 2006). Proteins containing this domain comprise a family (PF08774) belonging to the PD-(D/E)xK superfamily, which constitutes a large and functionally diverse group containing representatives involved in DNA replication (Holliday junction resolvases), restriction-modification, repair, and tRNA-intron splicing (Steczkiewicz *et al*, 2012). Members of this superfamily exhibit low sequence similarity but display a common fold in its enzymatic core (with $\alpha_1\beta_1\beta_2\beta_3\alpha_2\beta_4$ topology), which contains conserved residues (Asp, Glu, Lys) responsible for catalysis (Steczkiewicz *et al.*, 2012).

To gain insight into the molecular function of TseV2 and TseV3 and understand their phylogenetic relationship, we used TseV1, TseV2 and TseV3 (TseV4 is 79.1% identical to TseV3 and was not used) amino acid sequences as queries in JackHMMER searches (Potter *et al*, 2018) for four iterations on the NCBI nr database (November 4th, 2021) to fetch a total of 2254 sequences with significant similarity (inclusion threshold $\leq 10^{-9}$ and reporting threshold $\leq 10^{-6}$). Additional JackHMMER searches were performed using selected VRR-Nuc-containing proteins as queries (Bce1019, PmgM, T1p21,

KIAA1018, HP1472 and Plu1493) (Iyer *et al.*, 2006), and recently reported *bona fide* or putative T6SS effectors that also belong to the PD-(D/E)xK superfamily: TseT (Burkinshaw *et al.*, 2018); PoNe (Jana *et al.*, 2019); IdrD-CT (Sirias *et al*, 2020); TseTBg (Yadav *et al.*, 2021); Aave_0499 (Pei *et al.*, 2021); and $TseV^{PA}$ (Wang *et al*, 2021). A total of 39159 sequences were collected. For each JackHMMER dataset, we produced alignments with representatives from clusters formed by sequences displaying 80% coverage and 50-70% identity. These alignments were manually inspected, and divergent/truncated sequences were removed. We observed that the $\beta_2\beta_3\alpha_2\beta_4$ region of the enzymatic core was more conserved so we used this region for a new multiple sequence alignment to build a phylogenetic tree using maximum likelihood (Fig. 3A).

The resulting tree is composed of 9 main clades, with 5 of these clades comprising PmgM, T1p21, KIAA1018, Bce1019 and HP1472 that reproduce the classification proposed by Iyer et al. (2006) in which each of these clades constitutes a subfamily of the VRR-Nuc family (Fig. 3A, grey; Table S1). Bce1019 subfamily contains the endonuclease I from Bacteriophage T7 (PDB 1M0D) (Hadden *et al*, 2002) and the transposon Tn7 encoded nuclease protein TnsA from *E. coli* (PDB 1F1Z) (Hickman *et al*, 2000) (PDB 1T0F) (Ronning *et al*, 2004). The PmgM subfamily contains a nuclease with the same name from phage P1 (Iyer *et al.*, 2006). The T1p21 subfamily contains proteins encoded upstream of helicases (Iyer *et al.*, 2006). The KIAA1018 group includes the human Fanconi anemia-associated nuclease 1 (FAN1) (PDB 4REA) (PDB 4RIA) and its bacterial homolog *Pa*FAN1 (PDB 4R89), which are involved in DNA repair (Gwon *et al*, 2014; Wang *et al*, 2014; Zhao *et al*, 2014). Curiously, antibacterial T6SS effectors formed 4 groups (Fig. 3A, colors) in which TseV2 and TseV3 clustered with Plu1493 (Iyer *et al.*, 2006) and $TseV^{PA}$ (Wang *et al.*, 2021), whereas homologs of Aave_0499 (Pei *et al.*, 2021), IdrD (Sirias *et al.*, 2020) and PoNe (Jana *et al.*, 2019) formed separated clades

(Fig. 3A, colors; Table S1). These results indicate that TseV proteins are members of the Plu1493 subfamily (Iyer *et al.*, 2006). Conversely, homologs of TseT were too divergent to be grouped in the phylogenetic tree and impaired its reproducibility, thus indicating that they probably have a distinct evolutionary origin (Fig. S3; Table S1).

All T6SS effectors (TseVs, Aave_0499, IdrD and PoNe), except for TseT homologs, formed a clade with a bootstrap value higher than 75% (Fig. 3A, colors). The genomic context of TseV/Plu1493 homologs is different from the other VRR-Nuc family members (Table S2). While most of VRR-Nuc members (PmgM, T1p21, KIAA1018, Bce1019 and HP1472) are encoded next to genes involved in DNA metabolism, the gene neighborhood of antibacterial T6SS effectors (TseVs, Aave_0499, IdrD and PoNe) is enriched in proteins encoding components of the T6SS apparatus, adaptors, and immunity proteins (Fig. 3B; Table S2). In addition, we observed proteins containing domains of other secretion systems involved in biological conflicts, such as CdiB and POTRA (T5SS) and LXG (T7SS) domains (Fig. 3B; Table S2). Therefore, based on genomic context and biological function, we propose to name Plu1493-like subfamily the group formed by the clades containing TseVs, Aave_0499, IdrD and PoNe (Fig. 3A, colors).

Multiple amino acid sequence alignments from each clade revealed the conserved residues characteristic of the PD-(D/E)xK superfamily (Fig. 3C), which comprise the aspartic acid (D), glutamic acid (E) and lysine (K) that are part of the catalytic site responsible for hydrolyzing phosphodiester bonds (Steczkiewicz *et al.*, 2012). Using this information as a guide, substitution of the conserved aspartic acid for alanine in TseV2 and TseV3 ($TseV_{D282A}$ and $TseV3_{D230A}$) abrogated toxicity in *E. coli* (Fig. 3D). These results confirm that the enzymatic activity of the VRR-Nuc domain is essential for toxicity.

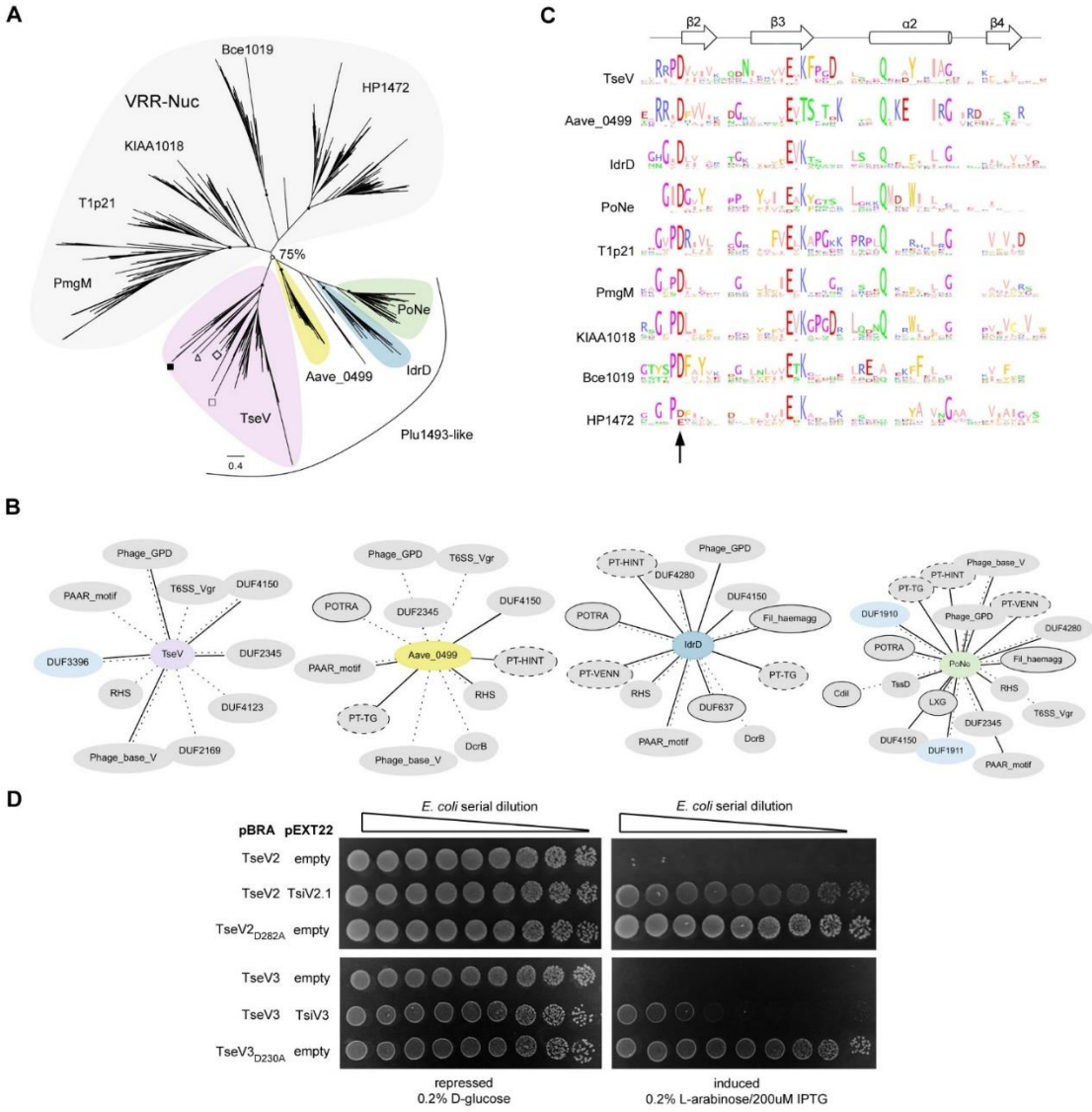

Fig. 3 VRR-Nuc-containing effectors are evolutionarily related to enzymes involved in DNA metabolism. (A) Maximum likelihood phylogenetic tree of VRR-Nuc family members (Bce1019, PmgM, T1p21, KIAA1018, HP1472, Plu1493) (Iyer *et al*., 2006) and recently reported bona fide or putative T6SS effectors belonging to the PD-(D/E)xK superfamily (TseT, PoNe, IdrD-CT, TseTBg, Aave_0499, TseV^{PA}). In the TseV clade (pink) the localization of TseV1 (□), TseV2 (Δ), TseV3 (■), and Plu1493 (◇) are marked. (B) Contextual network representation of domains and the genomic context of proteins belonging to Plu1493-like group (TseV, Aave_0499, IdrD, PoNe). Each circle represents a domain, which is either fused to (solid line) or encoded up- or downstream (dashed line) of the gene of interest (center). Borderless gray circles represent domains related to T6SS; bordered gray circles denote domains associated with a different bacterial secretion system; dashed nodes indicate pre-toxin domains; and light blue circles represent immunity proteins. (C) Sequence logo from the conserved $\beta_2\beta_3\alpha_2\beta_4$ of the PD-(D/E)xK enzymatic core from all clades shown in (A). The arrow indicates conserved aspartic acid that was mutated in (D). (D) *E. coli* toxicity assay. Serial dilution of *E. coli* containing pBRA and pEXT22 constructs, as indicated, spotted onto LB agar plates, and grown for 20 h. Images are representative of three independent experiments.

TseV2 and TseV3 induce cell death via DNA double-strand breaks

We set out to determine whether TseV2 and TseV3 could cause DNA damage by analyzing the activation of the SOS response - a stress response mechanism induced by the activation of RecA (recombinase protein A) in response to DNA damage (Walker, 1996). *E. coli* harboring the reporter plasmid pSC101-P_{recA}::GFP (Ronen *et al*, 2002), which carries the green fluorescent protein (GFP) under the control of the P_{recA} promoter, was co-transformed with either pBRA TseV2 or TseV3 and grown in AB media containing either 0.2% D-glucose or 0.2% L-arabinose (Fig. 4A and 4B). We observed an increase in GFP fluorescence when the expression of TseV2 or TseV3 was induced with L-arabinose, indicating the activation of the SOS response (Fig. 4A and 4B). To further assess the impact of TseV2 and TseV3 on bacterial chromosome stability, we used DAPI (4′,6-diamidino-2-phenylindole) to stain *E. coli* cells after inducing the expression of TseV2 or TseV3 for 1 h and evaluate nucleoid integrity by measuring the mean DAPI fluorescence per cell (Fig. 4C-F). Cells expressing TseV2 or TseV3 revealed smaller/degraded nucleoids and displayed reduced DAPI fluorescence (Fig. 4C-F), which indicates DNA degradation.

VRR-Nuc-containing enzymes have been shown to degrade 5’ flap single-strand DNA (Gwon *et al.*, 2014) and Holliday junctions (a four-way junction in which two DNA double-strands are held together) (Pennell *et al*, 2014). Expression of TseV2 and TseV3 in *E. coli* followed by genomic and plasmid DNA extraction failed to reveal any significant difference in DNA integrity between induced and repressed conditions after visualization via electrophoresis in agarose gels (data not shown). To evaluate whether TseV2 and TseV3 could induce a small number of DNA double-strand breaks that were not detected by electrophoresis, we used the reporter strain *E. coli* SMR14354 encoding a chromosomal GFP fused to the Gam protein from bacteriophage Mu (GamGFP) under

the control of the P_{tet} promoter (induced by tetracycline) (Shee *et al*, 2013). The Gam protein binds with high affinity and specificity to DNA double-strand ends, thus inducing the formation of GFP foci at specific sites (Shee *et al.*, 2013). *E. coli* SMR14354 carrying an empty pEXT20 plasmid or encoding either TseV2 or TseV3 were grown with 0.2% D-glucose (repressed) or with 200 μM IPTG (induced) and examined by fluorescence microscopy (Fig. 4G and 4H). Cells carrying an empty plasmid revealed an even distribution of GamGFP in the cytoplasm, with only a few foci representing spontaneous double-strand breaks (Fig. 4G and 4H). Conversely, *E. coli* expressing either TseV2 or TseV3 revealed several intense GFP foci in more than 80% and 75% of cells, respectively (Fig. 4G and 4H). Interestingly, the expression of TseV2 leads to the formation of fewer intense foci per cell, whereas the expression of TseV3 induces the development of several less intense foci per cell (Fig. 4G and 4H), suggesting that TseV3 might cleave DNA at more sites than TseV2. Together, these results reveal that TseV2 and TseV3 cause target cell death via specific DNA double-strand breaks.

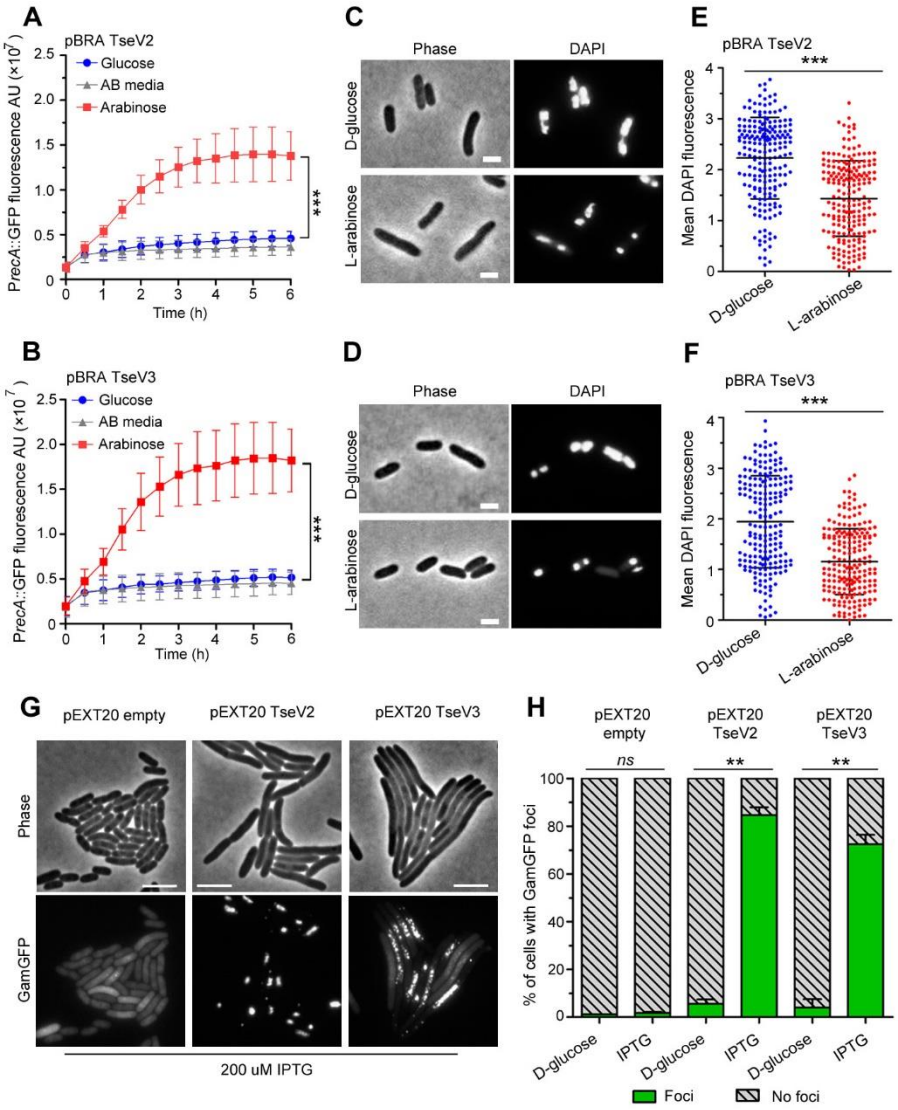

Fig. 4. TseVs induce target cell death via DNA double-strand breaks. (A-B) Activation of the SOS response was analyzed using *E. coli* cells harboring the reporter plasmid pSC101-P_{recA}::GFP and pBRA TseV2 (A) or pBRA TseV3 (B), which were grown in AB defined media with D-glucose or L-arabinose. Data is the mean ± SD of three independent experiments. ***p<0.001 (Student's *t* test). (C-D) Bright-field and DAPI images of *E. coli* cells carrying pBRA TseV2 (C) or pBRA TseV3 (D) grown in the presence of D-glucose (repressed) or L-arabinose (induced). Results are representative images of three independent experiments. (E-F) Quantification of the mean DAPI fluorescence per cell of 200 cells. Data correspond to the mean ± SD of a representative experiment. Scale bar 2 μm. ***p < 0.001 (Student's *t* test). (G) Representative bright-field and GFP images of *E. coli* co-expressing GamGFP and pEXT20 TseV2 or pEXT20 TseV3. Double-strand breaks appear as foci of GamGFP. Images are representatives of three independent experiments. Scale bar: 5 μm. (H) Quantification of the GamGFP foci shown in (G). Data are shown as the mean ± SD of the three independent experiments. **p < 0.01 (Student's *t* test).

TsiV3 interacts with the putative DNA-binding site of TseV3 to neutralize toxicity

To obtain information about the inhibitory mechanism of TsiV3, we decided to analyze whether this protein could directly interact with TseV3. Recombinant proteins were expressed, and the purified complex was analyzed using size exclusion chromatography coupled to multiple-angle light scattering (SEC-MALS) (Fig. S4). The MALS calculated average mass for the complex was 66.4 ± 3.3 kDa, which is close to the sum of the theoretical values of their monomers: 26.8 kDa and 37.4 kDa for 6xHis-TseV3 and TsiV3, respectively. SDS-PAGE analysis of the mixture confirmed the presence of 6xHis-TseV3 and TsiV3 (Fig. S4). These results reveal that TseV3 and TsiV form a 1:1 heterodimeric complex.

We were able to obtain crystals of the TseV3:TsiV3 complex, which belong to space group $P2_11$ and diffracted to a moderate resolution of 4 Å (Table S3). Matthews coefficient analysis indicated that two TseV3:TsiV3 complexes would be the most likely composition in the asymmetric crystal unit. We used AlphaFold (Jumper *et al*, 2021) models of $TseV3_{132-281}$ and $TsiV3_{10-327}$ for molecular replacement using Phaser (McCoy *et al*, 2007), which was able to place two copies of each monomer in the asymmetric unit with a final LLG (log-likelihood gain) of 486.87 and TFZ (translation function Z-score) of 12.4 - with both heterodimeric complexes adopting the same pose (our docked model is available using accession code ma-oyho8 at modelarchive.org). Therefore, the molecular replacement solution using the AlphaFold models most likely represents the correct relative orientation of the two subunits in the TseV3:TsiV3 complex (Fig. 5A). Given the relatively low resolution of the X-ray diffraction data, we chose not to refine these models against the processed dataset; however, our molecular replacement solution using the AlphaFold models was confirmed by identical placement using experimental PDB homologs taken from the DALI search described below - both TsiV and TsiT can be successfully utilized as search models for our experimental data, producing TFZ scores

of 8.3 and 9.2, respectively. Attempts to co-fold the TseV3 and TsiV3 complex with AlphaFold did not result in the extensive interface we observe in our experimentally docked single models, thus confirming the requirement for data-derived docking.

TsiV3 possesses a central β-sheet that is flanked by α-helices on one side and exposed on the other (Fig. 5A). This exposed β-sheet surface of TsiV3 binds to an α-β element of TseV3 that flanks its putative active site (composed of residues D_{230}, D_{245}, K_{247}) (Fig. 5A). In this configuration, the TseV3-interacting α-helix, which corresponds to the α_2 of the classical PD-(D/E)xK $\alpha_1\beta_1\beta_2\beta_3\alpha_2\beta_4$ core topology, projects its N-terminus towards the TsiV3 β-sheet (Fig. 5A).

Searches for structures similar to $TseV3_{132\text{-}281}$ and $TsiV3_{10\text{-}327}$ using the DALI server (Holm, 2020) revealed matches to proteins of related function: (a top Z-score of 33.5 for the immunity protein PA0821 PDB:7DRG and TsiV3; and a top Z-score of 3.8 between VRR-Nuc protein psNUC PDB:4QBL and TseV3). The modest RMSD (Root-Mean-Square Deviation) for the Cα positions in TseV3 and other VRR-Nuc enzymes indicates that TseV3 represents a variant of the VRR-Nuc family fold. Nevertheless, the PD-(D/E)xK consensus catalytic residues are identifiable as the modified sequence $MD_{230}IX_nD_{245}VK_{247}$ in TseV3. These residues are found in positions commensurate with active nucleases of the PD-(D/E)xK superfamily. Accordingly, superimposition of TseV3 with the well-characterized VRR-Nuc member *Pa*FAN1 (PDB 4R89) (Gwon *et al.*, 2014) (clade KIAA1018 in Fig. 3A) matches residues D_{230}, D_{245} and K_{247} of the former with residues D_{507}, E_{522}, and K_{524} of the latter (Fig. 5B).

*Pa*FAN1 (Gwon *et al.*, 2014) is the bacterial homolog of the human FAN1 (MacKay *et al*, 2010), which is involved in the repair of DNA damage such as interstrand cross-links (ICLs) (Gwon *et al.*, 2014; Jin *et al*, 2018). Human FAN1 is a structure-selective nuclease consisting of four domains: ubiquitin-binding zinc (UBZ); SAF-A/B,

Acinus and PIAS (SAP); tetratricopeptide repeat (TPR); and VRR-Nuc (Iyer *et al.*, 2006). Conversely, *Pa*FAN1 lacks the UBZ domain and contains an uncharacterized N-terminal domain (NTD), followed by SAP, TPR and VRR-Nuc (Iyer *et al.*, 2006; Gwon *et al.*, 2014). The structure of *Pa*FAN1 has been solved in complex with a 5' flap DNA substrate (PDB 4R89) (Fig. 5B, middle). As the catalytic residues of TseV3 align with those of *Pa*FAN1, we used the structure of the latter as a guide to analyze the likely mechanism by which TsiV3 may neutralize TseV3 activity. Comparison between the *Pa*FAN1:DNA and TseV3:TsiV3 complexes reveals that the path of the DNA substrate is potentially incompatible with the presence of TsiV3 (Fig. 5B). Hence, assuming the mode of substrate recognition is similar between *Pa*FAN1 and TseV3, this result suggests that the binding of TsiV3 sterically blocks the toxin active site. In our model of the complex, TsiV3 occlusion of the TseV3 active site would be enabled by TsiV3 loop, which projects into the putative TseV3 DNA-binding pocket (Fig. 5A, B).

To validate the accuracy of our TseV3:TsiV3 structural model, we designed point mutations to disrupt the interaction surface between the two proteins without perturbing the active site or its ability to bind DNA. Thus, residue P256 at the N-terminus of α_2 of TseV3 was replaced by lysine ($TseV3_{P256K}$), and residue L131 in the central β-sheet of TsiV3 was also replaced by lysine ($TsiV3_{L131K}$) (Fig. 5C). Native and mutated versions of the effector and immunity protein were co-transformed in *E. coli* to analyze toxicity (Fig. 5D). Results revealed that $TsiV3_{L131K}$ was unable to neutralize TseV3 toxicity. In addition, the mutated $TseV3_{P256K}$ maintained its enzymatic activity, displaying toxicity in *E. coli*; however, this mutant was not neutralized by co-expression with the native immunity protein (TsiV3) (Fig. 5D). Together, these results reinforce the accuracy of our model, which is comprised of both experimental constraints and theoretical model components.

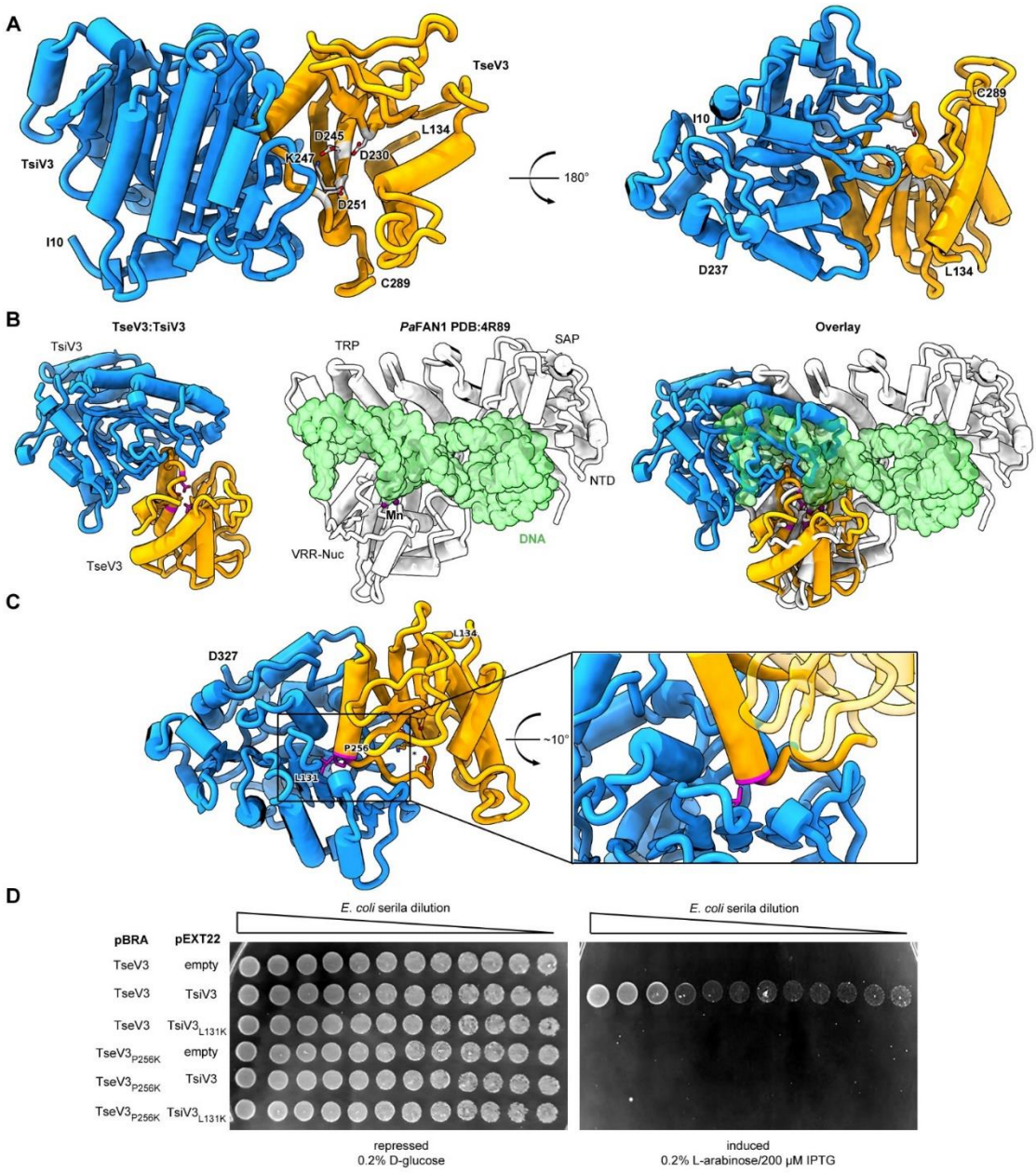

Fig. 5. The effector-immunity complex reveals that TsiV3 blocks TseV3 substrate-binding site. (A) Constrained model of the TseV3:TsiV3 heterodimer with two different views: TsiV3 in blue (I_{10}-D_{327}) and TseV3 in orange (L_{134}-C_{289}). Models are labeled to assist interpretation. PD-(D/E)xK superfamily conserved residues of TseV3 (D_{230}, D_{245}, and K_{247}) are shown in stick form and colored light grey, confirming that they converge to form a putative consensus active site. (B) Superimposition of the TseV3:TsiV3 coordinates with those of the *Pa*FAN1:DNA complex (PDB 4R89). *Pa*FAN1 protein in white, DNA duplex in green, and catalytic Mn^{2+} are depicted as purple spheres. The overlay (right) is presented in the same orientation as the individual complexes: TseV3:TsiV3 (left, catalytic residues in magenta) and *Pa*FAN1:DNA (middle). (C) Prediction of interface-compromising mutants in the TseV3:TsiV3 heterodimer. TsiV3 (blue) and TseV3 (orange) with putative active sites labeled with asterisk. Residues L_{131} of TsiV3 and P_{256} of TseV3 (both in stick form, magenta) form the closest point of contact in the heterodimer and are at the center of a hydrophobic-rich interface. (D) *E. coli* toxicity assay using

cells carrying plasmids with wild-type or point mutations in TsiV3 ($L_{131}K$) or TseV3 ($P_{256}K$) as a potential means to destabilize the TseV3:TsiV3 complex interaction.

Discussion

Bacterial antagonistic strategies targeting nucleic acids are very effective as these components are critical for life. In this study, we characterized a group of effectors containing the VRR-Nuc domain. This domain has not previously been reported to be used in biological conflicts (Zhang *et al.*, 2012), but recently was suggested to work as a T6SS effector due to its localization next to a PAAR protein in *P. aeruginosa* (Wang *et al.*, 2021) – for consistency we have decided to keep the name TseV for this group of effectors. Proteins containing the VRR-Nuc domain comprise a family (Iyer *et al.*, 2006) belonging to the PD-(D/E)xK superfamily, which contain a conserved enzymatic core composed by $\alpha_1\beta_1\beta_2\beta_3\alpha_2\beta_4$ (Steczkiewicz *et al*, 2012). The conserved catalytic residues (D, E, K) are located in the central $\beta_2\beta_3$-sheet, while the α_1-helix is associated with the formation of the active site and α_2-helix with substrate binding (Steczkiewicz *et al.*, 2012). Curiously, *S. bongori* encodes four TseV homologs: TseV2 and TseV3 are toxic in *E. coli*, whereas TseV1 and TseV4 are not toxic (Fig. 2). Based on what is known about the catalytic mechanism of PD-(D/E)xK nucleases, we hypothesize that the lack of α_2- and α_1-helix in TseV1 and TseV4, respectively, might explain the lack of toxicity (Fig. S5). Another curiosity is the presence of two homologs of the DUF3396 immunity genes downstream of both TseV2 and TseV1 (Fig. 2A). Such genomic organization is also conserved in other bacterial species like *Photorhabdus thracensis* (VY86_01065, VY86_01040), *Photorhabdus asymbiotica* (PAU_03539, PAU_03660) (Enterobacterales), *Marinobacter nauticus* (MARHY2492) (Pseudomonadales) and *Herbaspirillum huttiense* (E2K99_00955) (Burkholderiales). The fact that only one immunity protein (TsiV2.1) can neutralize the effector (TseV2) makes us wonder about

the role of the additional immunity protein gene - and why such genomic context is conserved. One possibility is that the extra immunity protein could regulate the effector at the transcriptional level as has been reported for the immunity protein TsiTBg known to regulate a different PD-(D/E)xK effector (TseTBg) (Yadav *et al.*, 2021).

The complexity of the PD-(D/E)xK superfamily and the rapid evolution of polymorphic toxins makes it difficult to categorize antibacterial effectors belonging to this group. However, our phylogenetic analysis was able to confidently group VRR-Nuc-containing effectors in one clade (TseV) and show that this group is different from the clades formed by the homologs of additional T6SS effectors (Aave_0499, IdrD, PoNe) (Fig. 3). Although proteins belonging to clades Aave_0499, IdrD, PoNe are not recognized by the Pfam model of VRR-Nuc, these proteins share similar genetic architectures concerning domain fusions and gene vicinity (Fig. 3B); therefore, we decided to call this larger group Plu1493-like to respect the original nomenclature proposed by Iyer et al. (2006).

The enzymatic activity of proteins belonging to the PD-(D/E)xK superfamily is quite diverse, but we were able to narrow down the possibilities and reveal that TseV effectors intoxicate target cells by inducing DNA double-strand breaks. Despite killing cells by the same mechanism, *E. coli* intoxicated by TseV2 and TseV3 display slight differences in phenotype. Due to the difference in GamGFP phenotype (Fig. 4G) and the number of resistant colonies obtained after ectopic expression of TseV2 and TseV3 in *E. coli* (Fig. S1), we hypothesize that the former cleaves DNA at fewer sites compared to the latter. It remains to be defined whether these effectors target a specific nucleotide sequence or recognize some conformational DNA structure. Unfortunately, whole genome sequencing of 20 resistant *E. coli* clones expressing the toxin (Fig. S1) failed to

uncover any evident mutation that could be attributed to the resistance phenotype (data not shown).

T6SSs effector-immunity complexes are related to type II toxin-antitoxin (TA) systems, which play several roles in bacterial physiology ranging from genomic stabilization and abortive phage infection to stress modulation and antibiotic persistence (Fraikin *et al*, 2020). Most T6SS immunity proteins described to date bind to effectors to regulate their enzymatic activity (Benz *et al*, 2012; Benz *et al.*, 2013; Dong *et al*, 2013; Li *et al*, 2013; Lu *et al*, 2014; Robb *et al*, 2016). An exception is Tri1 (type VI secretion ADP-ribosyltransferase immunity 1) from *Serratia proteamaculans*, which exhibits two modes of inhibition: active site occlusion and enzymatic removal of a post-translational modification (Ting *et al*, 2018). The neutralization mechanism of TsiT, which counteracts the PD-(D/E)xK effector TseT from *P. aeruginosa*, was also proposed to be different: TsiT interferes with the effector oligomerization state and hinders its nuclease activity (Wen *et al*, 2021). Our structural model of the TseV3:TsiV3 complex revealed that TsiV3 β-sheet binds to the α_2-helix of TseV3, which is involved in DNA binding in other PD-(D/E)xK members (Steczkiewicz *et al.*, 2012). In addition, the superposition of the TseV3:TsiV3 complex with the structure of *Pa*FAN1 bound to DNA confirms the hypothesis that TsiV3 likely occludes the substrate-binding site of TseV3.

It is estimated that *E. coli* and *Salmonella* diverged millions of years ago (Fookes *et al.*, 2011). *Salmonella*-specific functions are encoded by genes located in prophages and specific SPIs. Several characteristics of *S. bongori* suggest that this species may lie somewhere between *E. coli* and *S. enterica* during evolution (Christensen *et al*, 1998; Fookes *et al.*, 2011). Analyzing the synteny between *S.* Typhimurium 14028s and *S. bongori* NCTC 12419, we observed that the SPI-2 T3SS of *S. enterica* is localized in the equivalent genomic loci of the SPI-22 T6SS of *S. bongori* (Fig. S6). The SPI-2 T3SS of

S. enterica is well characterized for its importance during the intracellular stage of the infection cycle, allowing bacteria to manipulate host cellular functions and replicate (Hensel *et al*, 1995; Jennings *et al*, 2017). Whether the SPI-22 T6SS of *S. bongori* also works against eukaryotic cells remains to be established.

The genome of *S. bongori* NCTC 12419 encodes a large repertoire of orphan Hcp, VgrG and PAAR-like proteins (Fig. 1B) that are responsible for diversifying the array of effectors secreted by the SPI-22 T6SS. Conversely, the genome of *S.* Typhimurium 14028s that encodes a phylogenetically unrelated SPI-6 T6SS involved in competition with species of the gut microbiota (Sana *et al.*, 2016; Sibinelli-Sousa *et al.*, 2020) displays a restricted repertoire of orphan T6SS genes composed of only two Hcps (STM14_3785 and STM14_5414) (Blondel *et al.*, 2009). These observations suggest that the former bacterium may use its SPI-22 T6SS to target a greater variety of competitors, while the latter uses its SPI-6 T6SS to target a restricted number of species.

Here we add to the known diversity of antibacterial weapons, placing the VRR-Nuc family within the remit of T6SS effectors. Knowledge about the phylogeny and mechanism of action of this group of effectors will be important in interpreting its usage in other bacterial species, including the requirements of neutralization by very specific immunity pairings.

Material and Methods

Bacterial strains and growth conditions

A list of bacterial strains used in this work can be found in Table S4. Strains were grown at 37°C in Lysogeny Broth (10 g/L tryptone, 10 g/L NaCl, 5 g/L yeast extract) under agitation. Cultures were supplemented with antibiotics in the following

569 concentration when necessary: 50 μg/mL kanamycin, 100 μg/mL ampicillin, and 50
570 μg/mL streptomycin.

571 **Cloning and mutagenesis**

572 Putative effectors SBG_1828, SBG_1841, SBG_2718 and SBG_2723 were
573 amplified by PCR and cloned into pBRA vector under the control of P_{BAD} promoter
574 (Souza *et al*, 2015). Immunity proteins SBG_1828, SBG_1842, SBG_2719, SBG_2720,
575 SBG_2724 and SBG_2725 were cloned into pEXT22 under the control of P_{TAC} promoter
576 (Dykxhoorn *et al*, 1996). TseV2 and TseV3 were cloned in the pEX20 vector under the
577 control of P_{TAC} promoter (Dykxhoorn *et al.*, 1996) for GamGFP assays. For
578 complementation, SBG_1238 (TssB), SBG_1842 (TsiV3) and SBG_2724 (TsiV2.1)
579 were cloned into pFPV25.1 by replacing the GFP mut3 coding region for the genes of
580 interest (Valdivia & Falkow, 1996). Point mutations were created using QuikChange II
581 XL Site-Directed Mutagenesis Kit (Agilent Technologies) and pBRA TseV2 and pBRA
582 TseV3 plasmids as templates. S. *bongori* mutant strains were constructed by λ-Red
583 recombination engineering using a one-step inactivation procedure (Datsenko & Wanner,
584 2000). All constructs were confirmed by sequencing.

585 **Interbacterial competition assay**

586 Bacterial competition assays were performed using *S. bongori* (WT, Δ*tssB,*
587 Δ*tseV2/tsiV2.1/tsiV2.2* and Δ*tseV3/tsiV3*) as attackers, and *E. coli* K-12 W3110 carrying
588 pFPV25.1 Amp^R as prey. Overnight cultures of the attacker and prey cells were sub-
589 cultured in LB (1:30) until reaching $OD_{600ηm}$ 1.6, then adjusted to $OD_{600ηm}$ 0.4 and mixed
590 in a 10:1 ratio (attacker:prey), 5 μL of the mixture were spotted onto 0.22 μm
591 nitrocellulose membranes (1 × 1 cm) and incubated on LB agar (1.5%) at 37°C for the
592 indicated periods. Membranes containing the bacterial mixture were placed on 1.5 mL
593 tubes containing 1 mL of LB, homogenized by vortex, serially diluted, and plated on

selective plates containing antibiotics. The prey recovery rate was calculated by dividing the CFU (colony forming units) counts of the output by the CFU of the input.

E. coli toxicity assays

Overnight cultures of *E. coli* DH5α (LB with 0.2% glucose) carrying effectors (in pBRA) and immunity proteins (in pEXT22) were adjusted to $OD_{600ηm}$ 1, serially diluted in LB (1:4) and 5 µL were spotted onto LB agar plates containing either 0.2% D-glucose or 0.2% L-arabinose plus 200 µM IPTG – both supplemented with streptomycin and kanamycin - and incubated at 37°C for 20 h. For growth curves, overnight cultures of *E. coli* carrying pBRA TseV2 or TseV3 were inoculated in LB (1:50) with 0.2% D-glucose and grown at 37°C (180 rpm) for 1.5 h. Next, media was replaced with either fresh warm LB containing 0.2% D-glucose or 0.2% L-arabinose.

Microscopy Time-lapse studies

For time-lapse microscopy, LB agar (1.5%) pads were prepared by cutting a rectangular piece out of a double-sided adhesive tape, which was taped onto a microscopy slide as described previously (Bayer-Santos *et al*, 2019). *E. coli* DH5α harboring pBRA TseV2 or TseV3 were sub-cultured in LB (1:50) with 0.2% D-glucose until reaching $OD_{600ηm}$ 0.4-0.6 and adjusted to $OD_{600ηm}$ 1.0. Cultures were spotted onto LB agar pads supplemented either with 0.2% D-glucose or 0.2% L-arabinose plus antibiotics. Images were acquired every 15 min for 16 h using a Leica DMi-8 epifluorescent microscope fitted with a DFC365 FX camera (Leica) and Plan-Apochromat 63x oil objective (HC PL APO 63x/1.4 Oil ph3 objective Leica). Images were analyzed using FIJI software (Schindelin *et al*, 2012).

Bioinformatic analysis

Iterative profile searches using JackHMMER (Eddy, 2011) with a cutoff e-value of 10^{-6} and a maximum of four iterations were performed to search a non-redundant (nr)

protein database from the National Center for Biotechnology Information (NCBI) (Sayers *et al*, 2019). Similarity-based clustering of proteins was carried out using MMseqs software (Steinegger & Söding, 2017). Sequence alignments were produced with MAFFT local-pair algorithm (Katoh & Standley, 2013), and non-informative columns were removed with trimAl software (Capella-Gutiérrez *et al*, 2009). Approximately-maximum-likelihood phylogenetic trees were built using FastTree 2 (Price *et al*, 2010). Sequence logos were generated using Jalview (Waterhouse *et al*, 2009). HMM models were produced for each sequence alignment and compared against each other with the HH-suit package (Steinegger *et al*, 2019). Proteins were annotated using the HHMER package (Eddy, 2011) or HHPRED software (Söding *et al*, 2005) and Pfam (Bateman *et al*, 2004), PDB (Berman *et al*, 2007) or Scope (Fox *et al*, 2014) databases. An in-house Python script was used to collect the gene neighborhoods based on information downloaded from the complete genomes and nucleotide sections of the NCBI database (Sayers *et al.*, 2019).

TseV1-4 sequence alignments were produced with MAFFT local-pair algorithm (Katoh & Standley, 2013) and analyzed in AilView (Larsson, 2014) to separate the regions of interest. Sequence logos were produced using the Jalview (Waterhouse *et al.*, 2009). Protein structure predictions were performed with ColabFold (Mirdita *et al*, 2021) and AlphaFold (Jumper *et al.*, 2021), and visualization was performed using Pymol (DeLano, 2002).

The genome of *S. bongori* NCTC 12419 and *S.* Typhimurium NCTC 14028s were retrieved from the NCBI database and aligned with BLASTn (Camacho *et al*, 2009). The alignment was analyzed using Artemis Comparison Tool (ATC) (Carver *et al*, 2005). The genome map was constructed using the ATC plug-in DNAPlotter (Carver *et al*, 2009).

SOS response assays

644 Overnight cultures of *E. coli* DH5α harboring the reporter plasmid pSC101-
645 P_{recA}::GFP (Ronen *et al.*, 2002) and pBRA TseV2 or TseV3 were sub-cultured (1:50) in
646 LB with 0.2% D-glucose and grown at 37ºC until $OD_{600ηm}$ 0.4-0.6. Bacteria were
647 harvested and resuspended in AB defined media (0.2% $(NH_4)_2SO_4$, 0.6% Na_2HPO_4, 0.3%
648 KH_2PO_4, 0.3% NaCl, 0.1 mM $CaCl_2$, 1 mM $MgCl_2$, 3 µM $FeCl_3$) supplemented with 0.2%
649 sucrose, 0.2% casamino acids, 10 µg/mL thiamine and 25 µg/mL uracil (Bayer-Santos *et*
650 *al.*, 2019). Cells ($OD_{600ηm}$ 1.0) were placed in a black 96 well plate with clear bottom
651 (Costar) with 0.2% D-glucose or 0.2% L-arabinose to a final volume of 200 µL. GFP
652 fluorescence was monitored in a plate reader SpectraMax Paradigm Molecular Devices
653 for 6 h at 30°C.

654 **DAPI staining**

655 *E. coli* DH5α carrying pBRA TseV2 and TseV3 were sub-cultured in LB with
656 0.2% D-glucose (1:50) and grown at 37°C (180 rpm) until $OD_{600ηm}$ 0.4-0.6. Cells were
657 harvested and resuspended in new media with 0.2% D-glucose or 0.2% L-arabinose and
658 growth for an additional 1 h. Bacteria were fixed with 4% paraformaldehyde for 15 min
659 on ice, washed in phosphate buffer saline (PBS) and stained with DAPI (3 µg/mL) for 15
660 min at room temperature. Samples were washed once with PBS before transferring 1 µL
661 of each culture to a 1.5% PBS-agarose pad for visualization. Images were acquired in
662 Leica DMi-8 epifluorescent microscope fitted with a DFC365 FX camera (Leica) and
663 Plan-Apochromat 63x and 100x oil objectives (HC PL APO 63x and 100x/1.4 Oil ph3
664 objectives Leica). Images were analyzed using FIJI software (Schindelin *et al.*, 2012). To
665 assess DNA integrity, the mean pixel fluorescence per cell was manually measured from
666 200 bacteria from different fields from each experiment. The cell area was determined
667 using the bright field, and the mean pixel fluorescence per cell was measured in the DAPI
668 channel subtracting the background.

669 **DNA double-strand break microscopy**

670 *E. coli* SMR14354 containing a chromosomal GamGFP under the control of P_{tet}
671 promotor (Shee *et al.*, 2013) and harboring an empty pEXT20 or encoding TseV2 or
672 TseV3 were sub-cultured in LB (1:100) with 0.2% D-glucose grown for 1.5 h at 37°C
673 (180 rpm) before the induction of GamGFP with 50 ηg/mL tetracycline for 2 h. Bacteria
674 were resuspended in new media with either 0.2% D-glucose or 200 μM IPTG and grown
675 for 1 h. One microliter of each culture was spotted onto a 1.5% LB-agarose pad. Images
676 were acquired in a Leica DMi-8 epifluorescent microscope fitted with a DFC365 FX
677 camera (Leica) and Plan-Apochromat 100x oil objective (HC PL APO 100x/1.4 Oil ph3
678 objective Leica). Images were analyzed using FIJI software (Schindelin *et al.*, 2012). At
679 least 400 bacteria from each experiment were quantified.

680 **Protein expression and purification**

681 *E. coli* SHuffle cells carrying pRSFDuet 6xHis-TseV3-TsiV3 were grown in LB
682 supplemented with kanamycin (30°C, 180 rpm) until $OD_{600ηm}$ 0.4-0.6. Expression was
683 induced with 0.5 mM IPTG followed by incubation at 16°C for 16 h. Cells were harvested
684 via centrifugation at 9000 *g* for 15 min, and pellets were resuspended in buffer A (50 mM
685 Tris-HCl pH 7.5, 200 mM NaCl, 5 mM imidazole) and lysed at 4°C using an Avestin
686 EmulsiFlex-C3 homogenizer. The lysate was collected and centrifuged (48000 *g*) for 1 h
687 at 4 °C. The supernatant was loaded onto a 5 ml HisTrap HP cobalt column (GE
688 Healthcare) equilibrated in buffer A. The column was washed with 10 column volumes
689 (CV) of buffer A before running an elution gradient of 0-50% buffer B (50 mM Tris-HCl
690 pH 7.5, 200 mM NaCl, 500 mM imidazole) over 10 CV, followed by a final 10 CV wash
691 with 100% buffer B. The presence of TseV3-TsiV3 was confirmed by SDS-PAGE of
692 eluted fractions. TseV3-TsiV3 was concentrated using a Vivaspin® spin-concentrator

693 and further purified by size-exclusion chromatography on a Superdex 200 26/60 column
694 (GE Healthcare) equilibrated in 50 mM Tris-HCl pH 7.5, 150 mM NaCl.

695 SEC-MALS analyses were used to determine the molar mass of the TseV3-TsiV3
696 complex (concentration 3.2 mg/mL). Protein samples (400 µL injection volume) were
697 separated using a Superdex 200 10/300 column (GE Healthcare) equilibrated with buffer
698 (50 mM Tris-HCL pH 7.5, 20 mM NaCl) coupled to a miniDAWN TREOS multi-angle
699 light scattering system and an Optilab rEX refractive index detector. Data analysis was
700 performed using the Astra Software package version 7.1 (Wyatt TechnologyCorp).
701 Molecular mass was calculated assuming a refractive index increment dn/dc = 0.185
702 mL/g (Wen *et al*, 1996). Fractions were analyzed in SDS-PAGE to confirm protein
703 molecular weight.

704 **Crystallography and structure determination**

705 TseV3-TsiV3 was concentrated to 18 mg/mL and crystalized in 0.1 M HEPES pH
706 7.5 and 30 % v/v PEG Smear Low (12.5% v/v PEG 400, 12.5% v/v PEG 500,
707 monomethylether, 12.5% v/v PEG 600, 12.5% v/v PEG 1000). The crystals were
708 cryoprotected in the mother liquor supplemented with 20% ethylene glycol and
709 subsequently cryo-cooled in liquid nitrogen. X-ray diffraction data were collected at
710 Diamond Light Source on beamline i04, and initial data processing was performed using
711 the xia2-dials pipeline (Winter, 2010; Winter *et al*, 2018). The data were phased by
712 molecular replacement in Phaser (McCoy *et al.*, 2007) using AlphaFold (Jumper *et al.*,
713 2021) models of $TseV3_{134\text{-}289}$ and $TsiV3_{10\text{-}327}$, which were trimmed to include only the
714 high-confidence regions and omit the N-terminal DUF4150 domain of TseV3.

715 **Quantification and statistical analyses**

Statistical test, number of events, mean values and standard deviations are reported in each figure legend accordingly. Statistical analyses were performed using GraphPad Prism5 software and significance is determined by the value of $p < 0.05$.

Acknowledgements

We are grateful to Cristiane Rodrigues Guzzo for sharing reagents and equipment, and Alexandre Bruni Cardoso for allowing access to the fluorescence microscope. We thank members of the LEEP and EBS groups for scientific discussions. Crystallography analyses were performed at Diamond Light Source. This work was supported by São Paulo Research Foundation (FAPESP) grants to RFS (2016/09047-8), CSF (2017/17303-7) and EBS (2017/02178-2). AL is supported by Welcome Trust (209437/Z/17/Z). FAPESP fellowships were awarded to JTH (2018/25316-4), DESL (2019/22715-8), GGN (2021/03400-6), EEL (2019/12234-2), GSC (2020/15389-4), and EBS (2018/04553-8). LM is supported by a MIBTP studentship.

Author contributions

JTH, DESL and EBS outlined the study. JTH, DESL, EEL, GSC, and EBS performed experiments and analyzed data. LM and AL performed protein crystallography and analyzed data. GGN and RFS contributed with bioinformatic analyses. JTH, DESL, GGN, CSF, RFdS, RSG, AL and EBS contributed to the scientific discussions. JTH and EBS wrote the manuscript with input from other authors. All authors revised and approved the manuscript.

Conflict of interest

The authors declare no conflict of interest.

References

Alcoforado Diniz J, Coulthurst SJ (2015) Intraspecies competition in Serratia marcescens is mediated by type VI-secreted Rhs effectors and a conserved effector-associated accessory protein. *Journal of bacteriology* 197: 2350-2360

Bao H, Zhao J-H, Zhu S, Wang S, Zhang J, Wang X-Y, Hua B, Liu C, Liu H, Liu S-L (2019) Genetic diversity and evolutionary features of type VI secretion systems in Salmonella. *Future microbiology* 14: 139-154

Bateman A, Coin L, Durbin R, Finn RD, Hollich V, Griffiths-Jones S, Khanna A, Marshall M, Moxon S, Sonnhammer EL (2004) The Pfam protein families database. *Nucleic acids research* 32: D138-D141

Bayer-Santos E, Cenens W, Matsuyama BY, Oka GU, Di Sessa G, Mininel IDV, Alves TL, Farah CS (2019) The opportunistic pathogen Stenotrophomonas maltophilia utilizes a type IV secretion system for interbacterial killing. *PLoS pathogens* 15: e1007651

Benz J, Reinstein J, Meinhart A (2013) Structural insights into the effector–immunity system Tae4/Tai4 from Salmonella typhimurium. *PLoS One* 8: e67362

Benz J, Sendlmeier C, Barends TR, Meinhart A (2012) Structural insights into the effector–immunity system Tse1/Tsi1 from Pseudomonas aeruginosa. *PLoS One* 7: e40453

Berman H, Henrick K, Nakamura H, Markley JL (2007) The worldwide Protein Data Bank (wwPDB): ensuring a single, uniform archive of PDB data. *Nucleic acids research* 35: D301-D303

Blondel CJ, Jiménez JC, Contreras I, Santiviago CA (2009) Comparative genomic analysis uncovers 3 novel loci encoding type six secretion systems differentially distributed in Salmonella serotypes. *BMC genomics* 10: 1-17

Blondel CJ, Jiménez JC, Leiva LE, Álvarez SA, Pinto BI, Contreras F, Pezoa D, Santiviago CA, Contreras I (2013) The type VI secretion system encoded in Salmonella pathogenicity island 19 is required for Salmonella enterica serotype Gallinarum survival within infected macrophages. *Infection and immunity* 81: 1207-1220

Bondage DD, Lin J-S, Ma L-S, Kuo C-H, Lai E-M (2016) VgrG C terminus confers the type VI effector transport specificity and is required for binding with PAAR and adaptor–effector complex. *Proceedings of the National Academy of Sciences* 113: E3931-E3940

Brunet YR, Khodr A, Logger L, Aussel L, Mignot T, Rimsky S, Cascales E (2015) H-NS silencing of the Salmonella pathogenicity island 6-encoded type VI secretion system limits Salmonella enterica serovar Typhimurium interbacterial killing. *Infection and immunity* 83: 2738-2750

Burkinshaw BJ, Liang X, Wong M, Le AN, Lam L, Dong TG (2018) A type VI secretion system effector delivery mechanism dependent on PAAR and a chaperone–co-chaperone complex. *Nature microbiology* 3: 632-640

Camacho C, Coulouris G, Avagyan V, Ma N, Papadopoulos J, Bealer K, Madden TL (2009) BLAST+: architecture and applications. *BMC bioinformatics* 10: 1-9

Capella-Gutiérrez S, Silla-Martínez JM, Gabaldón T (2009) trimAl: a tool for automated alignment trimming in large-scale phylogenetic analyses. *Bioinformatics* 25: 1972-1973

Carver T, Thomson N, Bleasby A, Berriman M, Parkhill J (2009) DNAPlotter: circular and linear interactive genome visualization. *Bioinformatics* 25: 119-120

Carver TJ, Rutherford KM, Berriman M, Rajandream M-A, Barrell BG, Parkhill J (2005) ACT: the Artemis comparison tool. *Bioinformatics* 21: 3422-3423

Christensen H, Nordentoft S, Olsen JE (1998) NOTE: Phylogenetic relationships of Salmonella based on rRNA sequences. *International Journal of Systematic and Evolutionary Microbiology* 48: 605-610

Cianfanelli FR, Monlezun L, Coulthurst SJ (2016) Aim, load, fire: the type VI secretion system, a bacterial nanoweapon. *Trends in microbiology* 24: 51-62

Coulthurst S (2019) The Type VI secretion system: a versatile bacterial weapon. *Microbiology* 165: 503-515

789 Datsenko KA, Wanner BL (2000) One-step inactivation of chromosomal genes in Escherichia coli K-12
790 using PCR products. *Proceedings of the National Academy of Sciences* 97: 6640-6645

791 DeLano WL (2002) Pymol: An open-source molecular graphics tool. *CCP4 Newsletter on protein*
792 *crystallography* 40: 82-92

793 Dong C, Zhang H, Gao Z-Q, Wang W-J, She Z, Liu G-F, Shen Y-Q, Su X-D, Dong Y-H (2013) Structural
794 insights into the inhibition of type VI effector Tae3 by its immunity protein Tai3. *Biochemical Journal*
795 454: 59-68

796 Dykxhoorn DM, Pierre RS, Linn T (1996) A set of compatible tac promoter expression vectors. *Gene* 177:
797 133-136

798 Eddy SR (2011) Accelerated profile HMM searches. *PLoS computational biology* 7: e1002195

799 Fitzsimons TC, Lewis JM, Wright A, Kleifeld O, Schittenhelm RB, Powell D, Harper M, Boyce JD (2018)
800 Identification of novel Acinetobacter baumannii type VI secretion system antibacterial effector and
801 immunity pairs. *Infection and immunity* 86: e00297-00218

802 Fookes M, Schroeder GN, Langridge GC, Blondel CJ, Mammina C, Connor TR, Seth-Smith H, Vernikos
803 GS, Robinson KS, Sanders M (2011) Salmonella bongori provides insights into the evolution of the
804 Salmonellae. *PLoS pathogens* 7: e1002191

805 Fox NK, Brenner SE, Chandonia J-M (2014) SCOPe: Structural Classification of Proteins—extended,
806 integrating SCOP and ASTRAL data and classification of new structures. *Nucleic acids research* 42:
807 D304-D309

808 Fraikin N, Goormaghtigh F, Van Melderen L (2020) Type II toxin-antitoxin systems: evolution and
809 revolutions. *Journal of bacteriology* 202: e00763-00719

810 Gwon GH, Kim Y, Liu Y, Watson AT, Jo A, Etheridge TJ, Yuan F, Zhang Y, Kim Y, Carr AM (2014)
811 Crystal structure of a Fanconi anemia-associated nuclease homolog bound to 5′ flap DNA: basis of
812 interstrand cross-link repair by FAN1. *Genes & development* 28: 2276-2290

813 Hachani A, Allsopp LP, Oduko Y, Filloux A (2014) The VgrG proteins are "a la carte" delivery systems
814 for bacterial type VI effectors. *Journal of Biological Chemistry* 289: 17872-17884

815 Hadden JM, Déclais AC, Phillips SE, Lilley DM (2002) Metal ions bound at the active site of the junction-
816 resolving enzyme T7 endonuclease I. *The EMBO journal* 21: 3505-3515

817 Hensel M, Shea JE, Gleeson C, Jones MD, Dalton E, Holden DW (1995) Simultaneous identification of
818 bacterial virulence genes by negative selection. *Science* 269: 400-403

819 Hickman AB, Li Y, Mathew SV, May EW, Craig NL, Dyda F (2000) Unexpected structural diversity in
820 DNA recombination: the restriction endonuclease connection. *Molecular cell* 5: 1025-1034

821 Holm L (2020) Using Dali for protein structure comparison. In: *Structural Bioinformatics*, pp. 29-42.
822 Springer:

823 Iyer LM, Babu M, Aravind L (2006) The HIRAN domain and recruitment of chromatin remodeling and
824 repair activities to damaged DNA. *Cell Cycle* 5: 775-782

825 Jana B, Fridman CM, Bosis E, Salomon D (2019) A modular effector with a DNase domain and a marker
826 for T6SS substrates. *Nature communications* 10: 1-12

827 Jana B, Salomon D (2019) Type VI secretion system: a modular toolkit for bacterial dominance. *Future*
828 *microbiology* 14: 1451-1463

829 Jennings E, Thurston TL, Holden DW (2017) Salmonella SPI-2 type III secretion system effectors:
830 molecular mechanisms and physiological consequences. *Cell Host & Microbe* 22: 217-231

831 Jin H, Roy U, Lee G, Schärer OD, Cho Y (2018) Structural mechanism of DNA interstrand cross-link
832 unhooking by the bacterial FAN1 nuclease. *Journal of Biological Chemistry* 293: 6482-6496

833 Jumper J, Evans R, Pritzel A, Green T, Figurnov M, Ronneberger O, Tunyasuvunakool K, Bates R, Žídek
834 A, Potapenko A (2021) Highly accurate protein structure prediction with AlphaFold. *Nature* 596: 583-
835 589

836 Jurėnas D, Journet L (2021) Activity, delivery, and diversity of Type VI secretion effectors. *Molecular*
837 *Microbiology* 115: 383-394

838 Katoh K, Standley DM (2013) MAFFT multiple sequence alignment software version 7: improvements in
839 performance and usability. *Molecular biology and evolution* 30: 772-780

840 Kinch LN, Ginalski K, Rychlewski L, Grishin NV (2005) Identification of novel restriction endonuclease-
841 like fold families among hypothetical proteins. *Nucleic acids research* 33: 3598-3605

842 Koskiniemi S, Lamoureux JG, Nikolakakis KC, de Roodenbeke CtK, Kaplan MD, Low DA, Hayes CS
843 (2013) Rhs proteins from diverse bacteria mediate intercellular competition. *Proceedings of the*
844 *National Academy of Sciences* 110: 7032-7037

845 Larsson A (2014) AliView: a fast and lightweight alignment viewer and editor for large datasets.
846 *Bioinformatics* 30: 3276-3278

847 Leiman PG, Basler M, Ramagopal UA, Bonanno JB, Sauder JM, Pukatzki S, Burley SK, Almo SC,
848 Mekalanos JJ (2009) Type VI secretion apparatus and phage tail-associated protein complexes share a
849 common evolutionary origin. *Proceedings of the National Academy of Sciences* 106: 4154-4159

850 Li L, Zhang W, Liu Q, Gao Y, Gao Y, Wang Y, Wang DZ, Li Z, Wang T (2013) Structural Insights on the
851 bacteriolytic and self-protection mechanism of muramidase effector Tse3 in Pseudomonas aeruginosa.
852 *Journal of Biological Chemistry* 288: 30607-30613

853 Liang X, Pei T-T, Li H, Zheng H-Y, Luo H, Cui Y, Tang M-X, Zhao Y-J, Xu P, Dong T (2021) VgrG-
854 dependent effectors and chaperones modulate the assembly of the type VI secretion system. *PLoS*
855 *pathogens* 17: e1010116

856 Lu D, Zheng Y, Liao N, Wei L, Xu B, Liu X, Liu J (2014) The structural basis of the Tle4–Tli4 complex
857 reveals the self-protection mechanism of H2-T6SS in Pseudomonas aeruginosa. *Acta Crystallographica*
858 *Section D: Biological Crystallography* 70: 3233-3243

859 Ma J, Pan Z, Huang J, Sun M, Lu C, Yao H (2017a) The Hcp proteins fused with diverse extended-toxin
860 domains represent a novel pattern of antibacterial effectors in type VI secretion systems. *Virulence* 8:
861 1189-1202

862 Ma J, Sun M, Dong W, Pan Z, Lu C, Yao H (2017b) PAAR-Rhs proteins harbor various C-terminal toxins
863 to diversify the antibacterial pathways of type VI secretion systems. *Environmental microbiology* 19:
864 345-360

865 Ma L-S, Hachani A, Lin J-S, Filloux A, Lai E-M (2014) Agrobacterium tumefaciens deploys a superfamily
866 of type VI secretion DNase effectors as weapons for interbacterial competition in planta. *Cell host &*
867 *microbe* 16: 94-104

868 MacKay C, Déclais A-C, Lundin C, Agostinho A, Deans AJ, MacArtney TJ, Hofmann K, Gartner A, West
869 SC, Helleday T (2010) Identification of KIAA1018/FAN1, a DNA repair nuclease recruited to DNA
870 damage by monoubiquitinated FANCD2. *Cell* 142: 65-76

871 McCoy AJ, Grosse-Kunstleve RW, Adams PD, Winn MD, Storoni LC, Read RJ (2007) Phaser
872 crystallographic software. *Journal of applied crystallography* 40: 658-674

873 Mirdita M, Schütze K, Moriwaki Y, Heo L, Ovchinnikov S, Steinegger M (2021) ColabFold-Making
874 protein folding accessible to all.

875 Mougous JD, Cuff ME, Raunser S, Shen A, Zhou M, Gifford CA, Goodman AL, Joachimiak G, Ordoñez
876 CL, Lory S (2006) A virulence locus of Pseudomonas aeruginosa encodes a protein secretion apparatus.
877 *Science* 312: 1526-1530

878 Nguyen VS, Douzi B, Durand E, Roussel A, Cascales E, Cambillau C (2018) Towards a complete structural
879 deciphering of Type VI secretion system. *Current Opinion in Structural Biology* 49: 77-84

880 Pei T-T, Kan Y, Wang Z-H, Tang M-X, Li H, Yan S, Cui Y, Zheng H-Y, Luo H, Dong T (2021) Breaching
881 the cell-envelope barriers of gram-positive and fungal microbes by a type VI secretion system in
882 Acidovorax citrulli. *bioRxiv*

883 Pennell S, Déclais A-C, Li J, Haire LF, Berg W, Saldanha JW, Taylor IA, Rouse J, Lilley DM, Smerdon
884 SJ (2014) FAN1 activity on asymmetric repair intermediates is mediated by an atypical monomeric
885 virus-type replication-repair nuclease domain. *Cell reports* 8: 84-93

886 Peterson SB, Bertolli SK, Mougous JD (2020) The central role of interbacterial antagonism in bacterial life.
887 *Current Biology* 30: R1203-R1214

888 Petty NK, Bulgin R, Crepin VF, Cerdeño-Tárraga AM, Schroeder GN, Quail MA, Lennard N, Corton C,
889 Barron A, Clark L (2010) The Citrobacter rodentium genome sequence reveals convergent evolution
890 with human pathogenic Escherichia coli. *Journal of bacteriology* 192: 525-538

891 Pezoa D, Blondel CJ, Silva CA, Yang H-J, Andrews-Polymenis H, Santiviago CA, Contreras I (2014) Only
892 one of the two type VI secretion systems encoded in the Salmonella enterica serotype Dublin genome
893 is involved in colonization of the avian and murine hosts. *Veterinary research* 45: 1-9

894 Pissaridou P, 2018. Pseudomonas Aeruginosa Type Six Secretion System (T6SS): The Tse7 DNase
895 Effector and Post-translational Regulation of the H1-T6SS. Imperial College London.

896 Potter SC, Luciani A, Eddy SR, Park Y, Lopez R, Finn RD (2018) HMMER web server: 2018 update.
897 *Nucleic acids research* 46: W200-W204

898 Price MN, Dehal PS, Arkin AP (2010) FastTree 2–approximately maximum-likelihood trees for large
899 alignments. *PloS one* 5: e9490

900 Renault MG, Beas JZ, Douzi B, Chabalier M, Zoued A, Brunet YR, Cambillau C, Journet L, Cascales E
901 (2018) The gp27-like hub of VgrG serves as adaptor to promote Hcp tube assembly. *Journal of*
902 *molecular biology* 430: 3143-3156

903 Robb CS, Robb M, Nano FE, Boraston AB (2016) The structure of the toxin and type six secretion system
904 substrate Tse2 in complex with its immunity protein. *Structure* 24: 277-284

905 Ronen M, Rosenberg R, Shraiman BI, Alon U (2002) Assigning numbers to the arrows: parameterizing a
906 gene regulation network by using accurate expression kinetics. *Proceedings of the national academy of*
907 *sciences* 99: 10555-10560

908 Ronning DR, Li Y, Perez ZN, Ross PD, Hickman AB, Craig NL, Dyda F (2004) The carboxy-terminal
909 portion of TnsC activates the Tn7 transposase through a specific interaction with TnsA. *The EMBO*
910 *journal* 23: 2972-2981

911 Russell AB, Singh P, Brittnacher M, Bui NK, Hood RD, Carl MA, Agnello DM, Schwarz S, Goodlett DR,
912 Vollmer W (2012) A widespread bacterial type VI secretion effector superfamily identified using a
913 heuristic approach. *Cell host & microbe* 11: 538-549

914 Salih O, He S, Planamente S, Stach L, MacDonald JT, Manoli E, Scheres SH, Filloux A, Freemont PS
915 (2018) Atomic structure of type VI contractile sheath from Pseudomonas aeruginosa. *Structure* 26: 329-
916 336. e323

917 Sana TG, Flaugnatti N, Lugo KA, Lam LH, Jacobson A, Baylot V, Durand E, Journet L, Cascales E,
918 Monack DM (2016) Salmonella Typhimurium utilizes a T6SS-mediated antibacterial weapon to
919 establish in the host gut. *Proceedings of the National Academy of Sciences* 113: E5044-E5051

920 Sayers EW, Agarwala R, Bolton EE, Brister JR, Canese K, Clark K, Connor R, Fiorini N, Funk K, Hefferon
921 T (2019) Database resources of the national center for biotechnology information. *Nucleic acids*
922 *research* 47: D23

923 Schindelin J, Arganda-Carreras I, Frise E, Kaynig V, Longair M, Pietzsch T, Preibisch S, Rueden C,
924 Saalfeld S, Schmid B (2012) Fiji: an open-source platform for biological-image analysis. *Nature*
925 *methods* 9: 676-682

926 Schroll C, Huang K, Ahmed S, Kristensen BM, Pors SE, Jelsbak L, Lemire S, Thomsen LE, Christensen
927 JP, Jensen PR (2019) The SPI-19 encoded type-six secretion-systems (T6SS) of Salmonella enterica
928 serovars Gallinarum and Dublin play different roles during infection. *Veterinary microbiology* 230: 23-
929 31

930 Shee C, Cox BD, Gu F, Luengas EM, Joshi MC, Chiu L-Y, Magnan D, Halliday JA, Frisch RL, Gibson JL
931 (2013) Engineered proteins detect spontaneous DNA breakage in human and bacterial cells. *Elife* 2:
932 e01222

933 Shneider MM, Buth SA, Ho BT, Basler M, Mekalanos JJ, Leiman PG (2013) PAAR-repeat proteins sharpen
934 and diversify the type VI secretion system spike. *Nature* 500: 350-353

935 Sibinelli-Sousa S, Hespanhol JT, Nicastro GG, Matsuyama BY, Mesnage S, Patel A, de Souza RF, Guzzo
936 CR, Bayer-Santos E (2020) A family of T6SS antibacterial effectors related to l, d-transpeptidases
937 targets the peptidoglycan. *Cell reports* 31: 107813

Sirias D, Utter DR, Gibbs KA (2020) A family of contact-dependent nuclease effectors contain an exchangeable, species-identifying domain. *bioRxiv*

Söding J, Biegert A, Lupas AN (2005) The HHpred interactive server for protein homology detection and structure prediction. *Nucleic acids research* 33: W244-W248

Souza DP, Oka GU, Alvarez-Martinez CE, Bisson-Filho AW, Dunger G, Hobeika L, Cavalcante NS, Alegria MC, Barbosa LR, Salinas RK (2015) Bacterial killing via a type IV secretion system. *Nature communications* 6: 1-9

Steczkiewicz K, Muszewska A, Knizewski L, Rychlewski L, Ginalski K (2012) Sequence, structure and functional diversity of PD-(D/E) XK phosphodiesterase superfamily. *Nucleic acids research* 40: 7016-7045

Steinegger M, Meier M, Mirdita M, Vöhringer H, Haunsberger SJ, Söding J (2019) HH-suite3 for fast remote homology detection and deep protein annotation. *BMC bioinformatics* 20: 1-15

Steinegger M, Söding J (2017) MMseqs2 enables sensitive protein sequence searching for the analysis of massive data sets. *Nature biotechnology* 35: 1026-1028

Ting S-Y, Bosch DE, Mangiameli SM, Radey MC, Huang S, Park Y-J, Kelly KA, Filip SK, Goo YA, Eng JK (2018) Bifunctional immunity proteins protect bacteria against FtsZ-targeting ADP-ribosylating toxins. *Cell* 175: 1380-1392. e1314

Valdivia RH, Falkow S (1996) Bacterial genetics by flow cytometry: rapid isolation of Salmonella typhimurium acid-inducible promoters by differential fluorescence induction. *Molecular microbiology* 22: 367-378

Walker GC, 1996. The SOS response of Escherichia coli. Escherichia coli and Salmonella: cellular and molecular biology.

Wang J, Brackmann M, Castano-Diez D, Kudryashev M, Goldie KN, Maier T, Stahlberg H, Basler M (2017) Cryo-EM structure of the extended type VI secretion system sheath–tube complex. *Nature microbiology* 2: 1507-1512

Wang J, Yang B, Leier A, Marquez-Lago TT, Hayashida M, Rocker A, Zhang Y, Akutsu T, Chou K-C, Strugnell RA (2018) Bastion6: a bioinformatics approach for accurate prediction of type VI secreted effectors. *Bioinformatics* 34: 2546-2555

Wang R, Persky NS, Yoo B, Ouerfelli O, Smogorzewska A, Elledge SJ, Pavletich NP (2014) Mechanism of DNA interstrand cross-link processing by repair nuclease FAN1. *Science* 346: 1127-1130

Wang S, Geng Z, Zhang H, She Z, Dong Y (2021) The Pseudomonas aeruginosa PAAR2 cluster encodes a putative VRR-NUC domain-containing effector. *The FEBS Journal*

Waterhouse AM, Procter JB, Martin DM, Clamp M, Barton GJ (2009) Jalview Version 2—a multiple sequence alignment editor and analysis workbench. *Bioinformatics* 25: 1189-1191

Wen H, Liu G, Geng Z, Zhang H, Li Y, She Z, Dong Y (2021) Structure and SAXS studies unveiled a novel inhibition mechanism of the Pseudomonas aeruginosa T6SS TseT-TsiT complex. *International Journal of Biological Macromolecules* 188: 450-459

Wen J, Arakawa T, Philo JS (1996) Size-exclusion chromatography with on-line light-scattering, absorbance, and refractive index detectors for studying proteins and their interactions. *Analytical biochemistry* 240: 155-166

Winter G (2010) xia2: an expert system for macromolecular crystallography data reduction. *Journal of applied crystallography* 43: 186-190

Winter G, Waterman DG, Parkhurst JM, Brewster AS, Gildea RJ, Gerstel M, Fuentes-Montero L, Vollmar M, Michels-Clark T, Young ID (2018) DIALS: implementation and evaluation of a new integration package. *Acta Crystallographica Section D* 74: 85-97

Yadav SK, Magotra A, Ghosh S, Krishnan A, Pradhan A, Kumar R, Das J, Sharma M, Jha G (2021) Immunity proteins of dual nuclease T6SS effectors function as transcriptional repressors. *EMBO reports* 22: e51857

Zhang D, de Souza RF, Anantharaman V, Iyer LM, Aravind L (2012) Polymorphic toxin systems: comprehensive characterization of trafficking modes, processing, mechanisms of action, immunity and ecology using comparative genomics. *Biology direct* 7: 1-76

Zhang H, Gao Z-Q, Wang W-J, Liu G-F, Xu J-H, Su X-D, Dong Y-H (2013) Structure of the Type VI Effector-Immunity Complex (Tae4-Tai4) Provides Novel Insights into the Inhibition Mechanism of the Effector by Its Immunity Protein*[S]. *Journal of Biological Chemistry* 288: 5928-5939

Zhao Q, Xue X, Longerich S, Sung P, Xiong Y (2014) Structural insights into 5′ flap DNA unwinding and incision by the human FAN1 dimer. *Nature communications* 5: 1-9

Supplementary Figures

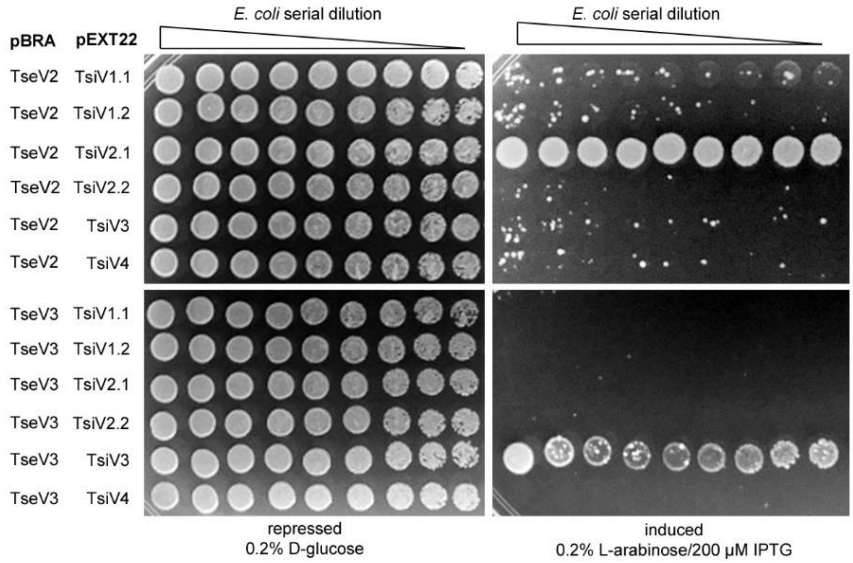

Fig. S1. Toxicity assay in *E. coli* co-transformed with pBRA TseV2 or pBRA TseV3 and the six different immunity proteins. Only one specific immunity could abrogate the toxic effect. Images are representative of three independent experiments.

Fig. S2. (A) Amino acid sequence alignment of VgrG1, VgrG2 and VgrG3. (B) Amino acid sequence alignment of VgrG2 and VgrG3. Amino acids are color-coded according to their properties.

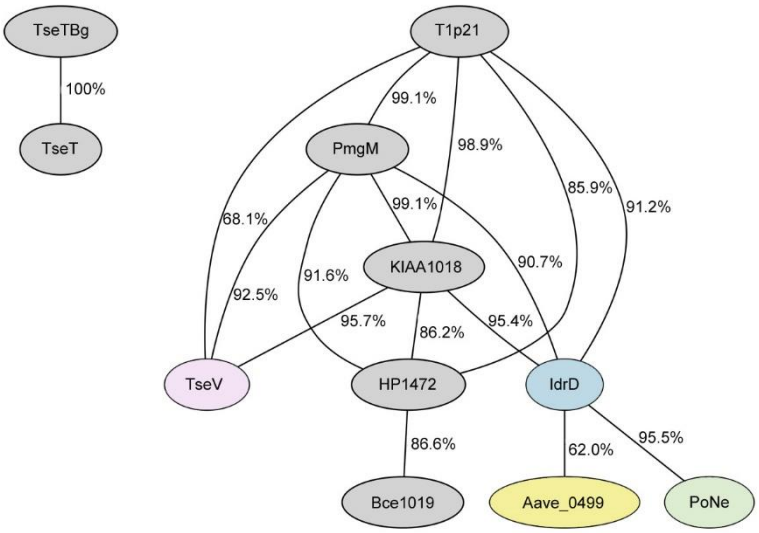

Fig. S3. Comparison of the HMM (Hidden Markov Model) from each clade shown in Fig. 3A. All clades present enough similarity to be clustered together, while the homologs of *P. aeruginosa* TseT and *B. gladioli* TseTBg differ from the other models.

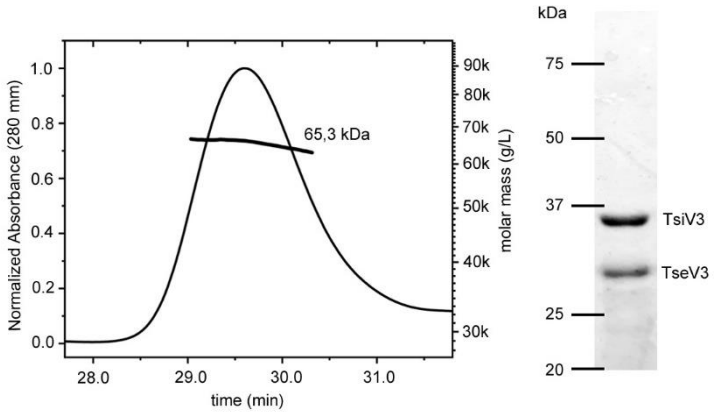

Fig. S4. SEC-MALS analysis shows the formation of a stable complex between TseV3:TsiV3. The line corresponds to the calculated molecular mass. Right panel: SDS-PAGE showing the apparent molecular mass of proteins eluted from SEC-MALS peak.

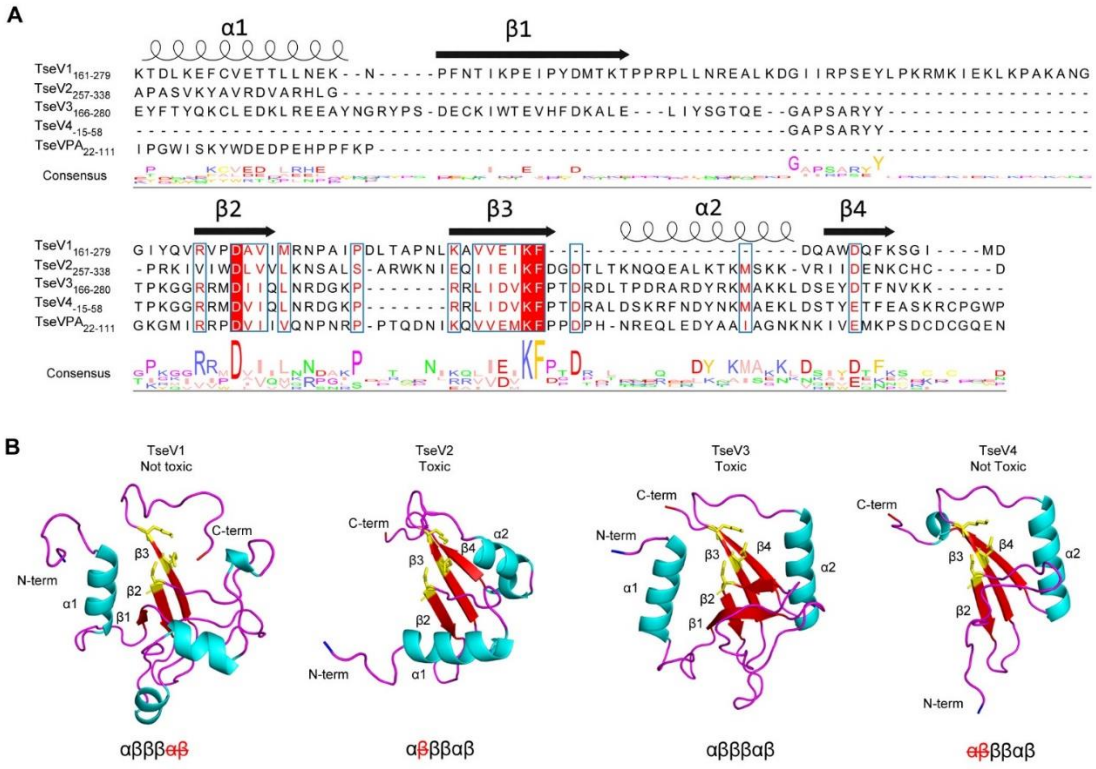

Fig. S5. (A) Manual amino acid sequence alignment of TseV1-4 and *P. aeruginosa* TseV (PA0822) based on secondary structures. The secondary structures are indicated above the alignments with α-helixes represented by spirals and β-sheets by arrows. The conserved catalytic residues are highlighted in red with the logo underneath the alignments. TseV4 contains another start codon located upstream of the annotated one. (B) TseV1-4 structures predicted by the AlphaFold (Jumper *et al.*, 2021). Underneath is the conserved PD-(D/E)xK enzymatic core with the absent structures marked in dashed red.

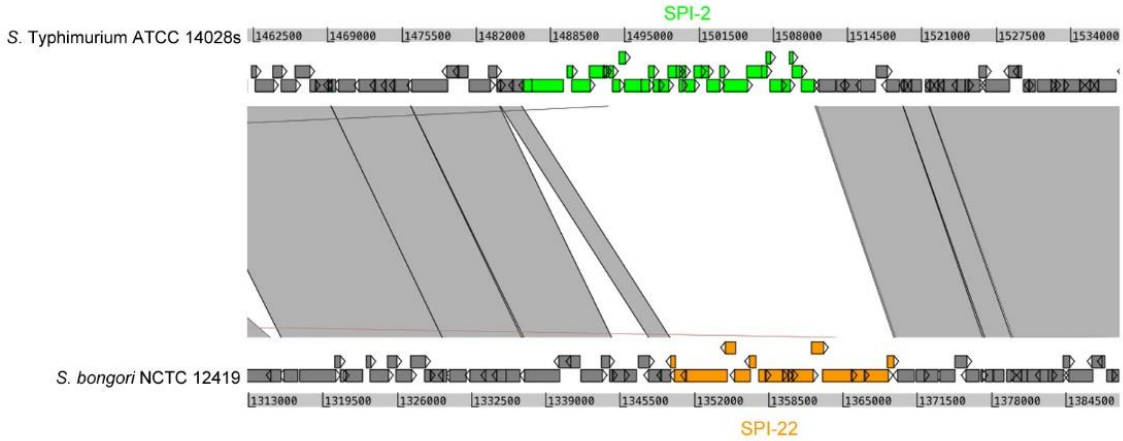

Fig. S6. Genomic alignment comparing *S.* Typhimurium and *S. bongori*. The regions encoding *S.* Typhimurium SPI-2 T3SS and *S. bongori* SPI-22 T6SS are in focus.

Supplementary Legends

Table S1A-J. List of all homologs collected by JackHMMER searches and used to build the phylogenetic tree shown in Fig. 3A.

Table S2A-J. List of genes surrounding representative sequences from each VRR-Nuc subfamily.

Table S3. Crystallographic statistics of the TseV3:TsiV3 complex.

Table S4. Strains, plasmids and primers used in the study.

Movie S1. Time-lapse microscopy of *E. coli* harboring pBRA TseV2 growing in media supplemented with 0.2% D-glucose. Timestamp in hh:mm. Scale bar: 5 μm. Arrows indicate selected bacteria shown in Fig. 2D.

Movie S2. Time-lapse microscopy of *E. coli* harboring pBRA TseV2 growing in media supplemented with 0.2% L-arabinose. Timestamp in hh:mm. Scale bar: 5 μm. Arrows indicate selected bacteria shown in Fig. 2D.

Movie S3. Time-lapse microscopy of *E. coli* harboring pBRA TseV3 growing in media supplemented with 0.2% D-glucose. Timestamp in hh:mm. Scale bar: 5 μm. Arrows indicate selected bacteria shown in Fig. 2D.

Movie S4. Time-lapse microscopy of *E. coli* harboring pBRA TseV3 growing in media supplemented with 0.2% L-arabinose. Timestamp in hh:mm. Scale bar: 5 μm. Arrows indicate selected bacteria shown in Fig. 2D.